Published online January 12, 2018

RESEARCH

Phenotypic Characterization, Fine Mapping, and Altered Expression Profiling of *Roses1* Mutation That Affects Organ Size and Water Loss Through Regulating Stomatal Density in Rice

Xiaoping Gong, Zhili Zhang, Junyang Yue, Wei Tang, Xiaofeng Tang, Zhengming Zeng, Xiangli Niu, Danyang Chen, Xianchun Sang, Fangming Xiao, Guanghua He,* and Yongsheng Liu*

ABSTRACT

Organ size is an important agronomic trait that directly affects the biomass of rice (*Oryza sativa* L.), thus identification and characterization of genes involved in organ size control would contribute to basic biology, as well as provide target genes for genetic manipulation of rice yield potential. Although organism or organ size is of pivotal importance, the molecular and genetic mechanisms underlying it remain far from understood. Here we report the isolation and characterization of *reduced organ size with early senescence1* (*roses1*) mutant in rice. The *roses1* mutant was obtained by ethyl methanesulfonate mutagenesis, and genetic analysis revealed that *roses1* mutation is controlled by a single recessive nuclear gene. Distinct reduction in the size of organs in *roses1* mutant plants was attributed to decreased cell number and cell size detected by histological analysis and the early leaf senescence with green and pale brown stripes, probably due to elevated stomata density detected by microscopy analysis. The *ROSES1* gene was isolated by using map-based cloning strategy, encoding a BEL1-like homeobox transcription factor containing a plant-specific peroxidase (POX) domain of unknown function. The β-glucuronidase (GUS) activity driven by the *ROSES1* promoter was strongly detected at the root meristem and elongation zone, shoot meristem, node, intercalary meristem of internode, leaf, inflorescence branch, and developing caryopsis and embryo. Differential gene expression analysis revealed potential regulatory networks involved in organ size control and stomata functioning that could be affected by the expression of the ROSES1 protein.

X. Gong, Z. Zeng, and Y. Liu, College of Life Sciences, Chongqing Univ., Chongqing 400030, China; X. Gong and Z. Zhang, Yudongnan Academy of Agricultural Sciences, Chongqing 408000, China; J. Yue, W. Tang, X. Tang, X. Niu, D. Chen, and Y. Liu, College of Food Science and Engineering, Hefei Univ. of Technology, Hefei 230009, China; W. Tang and Y. Liu, Ministry of Education Key Laboratory for Bio-resource and Eco-environment, College of Life Science, State Key Laboratory of Hydraulics and Mountain River Engineering, Sichuan Univ., Chengdu 610064, China; X. Sang and G. He, Rice Research Institute, Southwest Univ., Chongqing 400716, China; F. Xiao, Dep. of Plant, Soil, and Entomological Sciences, Univ. of Idaho, Moscow, ID 83844. X. Gong, Z. Zhang, and J. Yue contributed equally to this work. Received 27 Oct. 2016. Accepted 22 Aug. 2017. *Corresponding author (liu_ys@scu.edu.cn, hegh@swu.edu.cn). Assigned to Associate Editor Lee Tarpley.

Abbreviations: DEG, differentially expressed gene; DGE, differential gene expression; EMS, ethyl methanesulfonate; GFP, green fluorescent protein; GO, gene ontology; GUS, β-glucuronidase; LRI, Leaf-rolling index; OD_{649}, optical density at 649 nm; OD_{665}, optical density at 665 nm; PCR, polymerase chain reaction; POX, peroxidase; *roses1*, *reduced organ size with early senescence1*; SEM, scanning electron microscopy; SSR, simple sequence repeat; TEM, transmission electron microscopy; TF, transcription factor; WOX, WUSCHEL-related homeobox; WT, wild-type.

For multicellular organisms, growth and development continuously integrate the fundamental processes of cell proliferation, expansion, and differentiation with ever-changing environmental cues (Johansson et al., 2014). Although the final size of organs is affected by environmental stimuli, the developing organs possess intrinsic information to determine their final size (Mizukami, 2001; Sugimoto-Shirasu and Roberts, 2003; Tsukaya, 2003; Ingram and Waites, 2006; Tsukaya and Beemster,

Published in Crop Sci. 58:1–21 (2018).
doi: 10.2135/cropsci2016.10.0910

2006; Anastasiou and Lenhard, 2007). In animals, organ size is controlled by coordination of multiple cellular processes of cell growth, proliferation, and apoptosis. These processes are primarily regulated by two major pathways: the target of the rapamycin pathway and the Hippo pathway (Arsham and Neufeld, 2006; Dong et al., 2007; Pan, 2007; Zeng and Hong, 2008). In plants, organ growth up to its characteristic size is determined by cell number, cell size, or both that result from coordinated regulation of cell proliferation and cell expansion during organogenesis (Mizukami, 2001; Sugimoto-Shirasu and Roberts, 2003).

Several factors that promote plant organ growth by accelerating the primary cell proliferation have been described in plants, including AINTEGUMENTA (ANT), JAGGED (JAG), AUXIN-REGULATED GENE INVOLVED IN ORGAN SIZE (ARGOS), GROWTH-REGULATING FACTORS (AtGRFs), GRF-INTERACTING FACTORS (AtGIFs), KLUH/CYP78A5, GLUCOSE-6-PHOSPHATE TRANSPORTER (GPT2) (Krizek, 1999; Mizukami and Fischer, 2000; Hu et al., 2003; Kim et al., 2003; Dinneny et al., 2004; Kim and Kende, 2004; Ohno et al., 2004; Horiguchi et al., 2005; Anastasiou and Lenhard, 2007, Vercruyssen et al., 2015; Van Dingenen et al., 2016). By contrast, several regulators have been reported that negatively influence organ size by limiting the cell proliferation, such as CINCINNATA (CIN), AUXIN RESPONSE FACTOR 2 (ARF2), PPD1 and -2, STERILE APETALA (SAP), CINNAMOYL CoA REDUCTASE (CCR1) (White, 2006; Xue et al., 2015; Wang et al., 2016b).

Plant organ size is also regulated by cell expansion. A relatively large number of factors have been described to regulate organ growth by promoting cell expansion, such as P450 ROTUNDIFOLIA 3 (ROT3), ANGUSTIFOLIA (AN), ARGOS-LIKE (ARL) (Tsuge et al., 1996; Kim et al., 1998, 1999, 2002; Cho and Cosgrove, 2000; Hu et al., 2006), SMALL AUXIN UP-RNA (SAUR) (Spartz et al., 2014), ORGAN SIZE RELATED 2 (OSR2) (Qin et al., 2014), KUODA1 (KUA1) (Lu et al., 2014a), AtEXPA1 (Zhang et al., 2010), AtEXP10, POM-POM2 (cellulose synthase interacting 1) (Bringmann et al., 2012), auxin binding protein1 (ABP1) (Chen et al., 2014; Paque et al., 2014), EXIGUA (Rubio-Díaz et al., 2012), XETs and XTHs (Sasidharan et al., 2010), AtPGLs (Park et al., 2015), cell wall-associated kinases (WAKs) (Kohorn, 2016), Fragile Fiber1 (FRA1) (Zhu et al., 2015), PROFILIN1 (PRF1, a conserved actin monomer-binding protein) (Cao et al., 2016), CESA3 S211 and T212 (Chen et al., 2016), QUASIMODO2 (QUA2) (Mouille et al., 2007), Ca^{2+}/H^{+}-antiporter (CAX1) (Conn et al., 2011), *Arabidopsis thaliana* (L.) Heynh. homeobox 12 (ATHB12) (Hur et al., 2015), NGATHA (NGA) (Ballester et al., 2015), ABCB19 (an ATP-binding cassette membrane protein required for polar auxin transport) (Wu et al., 2016), myosins (motor proteins) (Peremyslov et al., 2015), BRI1-EMS-SUPPRESSOR1 (BES1) (Jiang et al., 2015), RLP44 (a receptor-like protein) (Wolf et al., 2014), PSKR1 (a leucine-rich repeat receptor kinase for phytosulfokine) (Ladwig et al., 2015), Cotton (*Gossypium hirsutum* L.) Golgi-Related 2 and 3 (CGR2 and -3) (Weraduwage et al., 2016), SPIRAL1 (SPR1, the microtubule plus-end tracking protein) (Nakajima et al., 2004; Galva et al., 2014), augmin complex (Liu et al., 2014), SNARE (soluble N-ethylmaleimide-sensitive factor attachment protein receptor)/AtVAM3/AtVTI11/SYP121/122 (Yano et al., 2003; Löfke et al., 2015), SEC11/KEULE (Karnik et al., 2015), ZmABA8ox1b (Li et al., 2016), and ADP-ribosylation factor (ZmArf2) (Wang et al., 2016a). By contrast, several factors were shown to control organ growth by negatively regulating cell expansion, including BIGPETALp (BPEp), RPT2a (Szécsi et al., 2006; Kurepa et al., 2009; Sonoda et al., 2009), MULTIPASS (OsMPS, an R2R3-type MYB transcription factor [TF]) (Schmidt et al., 2013), PEROXIDASE71 (AtPRX71) (Raggi et al., 2015), Sl-IAA17 (Aux and IAA transcriptional repressor) (Su et al., 2014), KNOPE1 (KNOTTED-like) (Testone et al., 2015), AtKINESIN-13A (AtKIN13A) (Fujikura et al., 2014), and rapid alkalinization factor (RALF) (Pearce et al., 2001; Bergonci et al., 2014).

In addition, several defined regulators have been demonstrated to be involved in organ size control by regulating both cell expansion and cell number, such as CYCA2;1 (Polko et al., 2015), DA1 (Nath et al., 2003), MED25/ENHANCER OF DA1 (EOD1)/BIG BROTHER (Li et al., 2008; Xia et al., 2013), SUPPRESSOR OF DA1/UBIQUITIN SPECIFIC PROTEASE 15 (UBP15) (Xu and Li, 2011; Du et al., 2014). Intriguingly, cell proliferation and cell expansion can compensate each other to influence final organ size. In this case, plant organ size is either synergistically or reversely determined by cell proliferation and cell expansion. For example, pytochrome B, phytochrome-interacting factors (Johansson et al., 2014), AAA ATPase (RPT2a) (Kurepa et al., 2009), H^{+}-PPase/ECH2 (Katano et al., 2016), and CYCD3;1 (Randall et al., 2015) were characterized in regulating organ size by compromising cell number and cell expansion in response to intrinsic or environmental cues.

Here we report the isolation and functional characterization of a *reduced organ size with early senescence* (*roses1*) mutant in rice (*Oryza sativa* L.). Phenotypic characterization and map-based cloning demonstrate that *ROSES1* encodes a homeobox domain protein that positively controls organ size through regulating cell number and cell expansion. Loss-of-function of *roses1* mutation results in an increased stomatal density and gives rise to precocious senescence with underdeveloped chloroplast

and reduced photosynthesis. Molecular cloning of the *ROSES1* gene helps us further understand the physiological roles of homeobox TF with plant-specific peroxidase (POX) domain in cell proliferation and cell expansion, as well as in response to environmental clues.

MATERIALS AND METHODS

Plant Materials and Growth Conditions

The *roses1* mutant was isolated from an *O. sativa* subsp. *indica* cultivar Fuhui9802 that was treated by ethyl methanesulfonate (EMS). Fuhui9802, an elite restorer line of hybrid rice, was bred by the Yudongnan Academy of Agricultural Sciences, Chongqing, China. After multiple generations of inbreeding, the homozygous *roses1* mutant line showing reduced organ size, and green-brown striped early senescence was obtained. To dissect the inheritance of a *roses1* mutation, homozygous *roses1* mutant plants were pollinated by two typical *indica* cultivars, ZhongjiuB and Q4B, respectively. The F_1 seeds were sown and transplanted as individual plants to generate F_2 segregating populations by inbreeding (Rao et al., 2015). The numbers of individuals showing wild-type (WT) and *roses1* mutant phenotypes were scored, and the segregation ratio of WT versus *roses1* mutation was determined at the tillering stage. Genetic analysis was performed on *roses1*, and recessive individuals showing a *roses1* mutant phenotype were retrieved for preliminary mapping of the mutation. The *roses1* mutation was fine mapped in the F_2 population from the cross between *roses1* and ZhongjiuB. All the plants, including the WT Fuhui9802, *roses1* mutants ZhongjiuB and Q4B, and the mapping population, were planted on the farm of Chongqing University, China.

Measurements of Agronomic Traits

Important agronomic traits were measured using the mature WT Fuhui9802 and *roses1* plants, including plant height, length of internodes, flag leaf length and width, effective panicle number per plant, panicle length, grain number per panicle, filled grain number per panicle, seed set frequency, grain weight, seed length, and seed width (Guo et al., 2014).

Physiological Analysis

At the heading stage, stomatal conductance, photosynthetic rate, and transpiration rate in the WT Fuhui9802 and *roses1* plants were determined using LI-6400 portable photosynthesis meter (LiCor) according to the manufacturer's instructions (Guo et al., 2014). 0.5 g of well-developed leaves were detached from the WT or *roses1* plants at three developmental stages (20, 60, and 90-d grown in the irrigated field after germination). Leaf tissues were incubated with 20 mL 95% ethanol in dark for 12 h. The extract was further diluted five-fold with 95% ethanol, and its optical density was read at 665 and 649 nm (denoted as OD_{665} and OD_{649}) in an ultraviolet spectrometer (Unico, UV-2100) with 95% ethanol serving as the control. The pigment concentrations were calculated according to the following formulas (Bao and Leng, 2005; Lu et al., 2014b): chlorophyll a content (mg L^{-1}) = $13.95OD_{665} - 6.88OD_{649}$, chlorophyll b content (mg L^{-1}) = $24.96OD_{649} - 7.32OD665$, and total chlorophyll (mg L^{-1}) = chlorophyll a + chlorophyll b. Pigment content of samples (mg g^{-1}) = $1000\rho V(N/m)$, where ρ is colorimetric liquid pigment content of sample (mg L^{-1}), V is extraction volume (mL), N it the sample dilution multiple, m is sample fresh weight or dry weight (g), and 1000 is the coefficient that converts milliliters into liters.

Determination of Leaf Rolling Indices

The WT Fuhui9802 and *roses1* mutant rice plants were grown in a paddy field during the rice growing season. At the tillering stage, the plants were transferred to pots in the artificial climate incubators for 2 wk to acclimate the plants to incubator growth conditions. The growth conditions in the artificial climate incubators were set up as follows: 12 h light (300 μmol m^{-2} s^{-1}) at 30°C and 12 h dark at 22°C with 60% relative humidity. Then, the plants were treated with different growth temperatures as follows: 2 h light (300 μmol m^{-2} s^{-1}) with 60% relative humidity, for 22, 24, 28, 30, 32, 36, and 38°C, respectively, to test the opening levels of rice stomata. Leaf width (Lw) was defined as the greatest width of the flattened leaf blade. The natural distance between the leaf margins of the rolled blade (Ln) was also measured and used to calculate leaf rolling indices (LRIs) as LRI (%) = (Lw − Ln)/Lw × 100 (Shi et al., 2007).

Microscopy Analysis

Stomatal density and aperture were measured using scanning electron microscopy (SEM), as described previously (Zhang et al., 2011). Leaves of 4-wk-old plants treated with 20% PEG6000 for 18 d were detached and immediately fixed by 2.5% glutaraldehyde in 0.1 M phosphate buffer (pH 7.2) at 4°C for 24 h, washed twice with 0.1 M phosphate buffer for 10 min, and then fixed samples were dehydrated with gradual ethanol series (immersed in 50, 60, 70, 80, 90, and 100% ethanol sequentially for 10 min each). After drying in a vacuum dryer, the samples were sprayed with gold powder and examined under a scanning electron microscope (Hitachi S-450). Three plants of the WT and *roses1* were used as samples for analysis of leaf stomatal parameters with SEM. More than 20 measurements (20 measurements for testing the stomata length, 150 measurements for testing the opening levels of rice stomata) in different parts of the sample were conducted to determine the average values of concentrations.

To analyze pollen development, pollen sampled before flowering from spikelets of WT Fuhui9802 and *roses1* plants was stained with 1% (w/v) iodine and potassium iodide (I_2–KI) solution for a viability assay (Yang et al., 2011). The stained pollen grains were then visualized and images were recorded using a Nikon E600 microscope.

For section analysis, leaves and the second internode to the top of the WT and *roses1* mutant were collected, fixed overnight by 50% ethanol, 0.9 M glacial acetic acid, and 3.7% formaldehyde at 4°C, dehydrated with a graded ethanol series, infiltrated with xylene, and embedded in paraffin (Sigma). Three plants of the WT and *roses1* mutant were used for sampling leaves and culms. The 8-μm-thick sections were transferred onto poly-L-Lys-coated glass slides, deparaffinized in xylene, and dehydrated through an ethanol series. The transverse sections and longitudinal sections were stained sequentially with 1% safranine (Amresco) and 1% fast green (Amresco) and were then dehydrated

through an ethanol series, infiltrated with xylene, and finally mounted beneath a cover slip. Light microscopy was performed using a Nikon E600 microscope (Ren et al., 2013). The size of leaf bulliform cells, culm cells, and pollen cells, as well as chloroplast compartment size of mesophyll cells, were measured using the ImageProPlus software (Media Cybernetics, 2006).

Transmission electron microscopy (TEM) was used to determine the chloroplast structure in *roses1* and WT leaves at the heading stage, as described previously (Fang et al., 2010). Three samples from the middle part of flag leaf of WT plants, green portion of pale brown striped flag leaf, and brown portion of pale brown striped flag leaf of *roses1* plants were fixed in primary fixative solution (2.5% glutaraldehyde) and then post-fixed for 2 h with 1% osmium tetroxide after washing with 0.1 mol L^{-1} phosphate-buffered saline. Tissues were stained using uranyl acetate, dehydrated in ethanol, and embedded in Spur's medium before sectioning. Samples were stained and examined using an H-7500 instrument (Hitachi, Japan) for TEM.

Water Loss Rate

To determine if leaf water loss rate was related to the dynamic rolling of *roses1* leaves under an increment of environmental temperatures, water loss rate in the plants was measured according to the method reported previously with minor modifications (Cui et al., 2008). The first, second, and third fully expanded leaves from topmost leaf of 14-wk-old plants were excised, and their fresh weights were immediately measured, then placed on open Petri dishes at 2°C and 48% relative humidity. The water loss of each leaf was determined by weighing at 30-min intervals for 2.5 h. Leaf water loss rate was calculated as the weight of water loss at each interval divided by the initial leaf weight.

Molecular Mapping of *roses1*

Bulked segregation analysis was employed for linkage analysis (Michelmore et al., 1991). Total DNA of the parental lines or DNA bulk was extracted using the cetyl trimethyl ammonium bromide method (Murray and Thompson, 1980), whereas genomic DNA of F_2 individuals was isolated using an alkaline extraction method (Sang et al., 2006). Simple sequence repeat (SSR) markers (Supplemental Table S1, derived from the Gramene website based on the SSR linkage map constructed by McCouch et al., 2002) were synthesized by the Shanghai Invitrogen Company, China. The total polymerase chain reaction (PCR) volume was 12.6 μL and contained the following components: 1.25 μL 10× PCR buffer, 1 μL of 50 ng μL^{-1} DNA, 0.75 μL of 25 mmol L^{-1} $MgCl_2$, 0.5 μL of 2.5 mmol L^{-1} deoxynucleotides, 8 μL of double-distilled H_2O, and 0.1 μL of 5 U μL^{-1} Taq DNA polymerase (Sangon Biotech). Amplification was performed on a MyCycler Thermal Cycler (Bio-Rad) under the following conditions: denaturing at 94°C for 5 min, followed by 35 cycles of denaturing at 94°C for 30 s, annealing at 55°C for 30 s, extension at 72°C for 1 min, and a final extension for 10 min at 72°C. Amplified products were separated by electrophoresis on 10.0% polyacrylamide gels, and the band patterns were visualized using the silver staining protocol (Luo et al., 2007). For linkage map construction, all individual F_2 plants, derived from the cross between ZhongjiuB and *roses1*, with reduced organ size and green-brown striped early senescence leaves were used to construct a linkage map. Recessive F_2 individuals showing banding patterns similar to those of ZhongjiuB were designated as A, individuals similar to those of *roses1* were designated as B, and the F_1 hybrid between ZhongjiuB and *roses1* was designated as H. Genetic distances were calculated with the formula $[(H + 2A)/2n] \times 100$, where H is the number of H-type plants, A is the number of A-type plants, and n is the total number of F_2 recessive individuals used to map *roses1*. The gene mapping involved 512 pairs of SSR markers.

Quantitative Real-Time Polymerase Chain Reaction

Total RNA from leaves of the WT Fuhui9802 and *roses1* mutant was extracted at the tillering stage using an RNA prep pure plant kit (Tiangen). The first strand of complementary DNA was synthesized from 2 μg of total RNA using oligo$(dT)_{18}$ primers in a 25-μL reaction volume using the SuperScript III Reverse Transcriptase Kit (Invitrogen). The quantitative real-time PCR analysis was performed with an ABI Prism 7000 Sequence Detection System and the SYBR Supermix Kit (Bio-Rad), and each sample was amplified in triplicate. The primers used for the quantitative real-time PCR assay are listed in Supplemental Table S1.

Phylogenetic Analyses

The amino acid sequence of the ROSES1 protein was used as bait for a homology with the BLASTN program (Altschul et al., 1997) search against the nonredundant database on the National Center for Biotechnology Information (NCBI) website. More than 100 blast hits were obtained, and 23 protein sequences of the top hits among different species were selected to construct a phylogenetic tree after multiple alignment (Supplemental Table S2). Maximum likelihood phylogenetic analysis was performed by MEGA7.0 using the neighbor-joining method (Kumar et al., 2016). The bootstrap test was replicated 1000 times.

Subcellular Localization of the ROSES1 Protein

The complementary DNA sequence of *ROSES1* was amplified using the specific primers ROSES1gfpF and ROSES1gfpR (Supplemental Table S1). This complementary DNA was fused in frame with green fluorescent protein (GFP) in vector pCAMBIA1301 (GenBank accession AF234297; Center for the Application of Molecular Biology of International Agriculture, Black Mountain, QLD) with minor modifications to generate the transient expression construct *35S::GFP-ROSES1*. The *35S::GFP-ROSES1* plasmids were transferred into *Agrobacterium tumefaciens* Smith & Townsend strain EHA105 by electroporation. The tobacco (*Nicotiana tabacum* L.) epidermal cells were transformed according to a previously described method (Xiao et al., 2007).

Promoter-GUS Analysis

For promoter-β-glucuronidase (GUS) fusion studies, a 3.1-kb genomic DNA fragment that contained the promoter region of the *roses1* gene was amplified by PCR using specific primers (Supplemental Table S1) and then cloned into vector pCAMBIA1301 (Cambia), which resulted in a fusion of the *ROSES1* promoter and the GUS reporter gene. The *pROSES1::GUS* construct was transformed into Fuhui9802 by

the *A. tumefaciens*-mediated transformation method (Tinland, 1996). About 12 independent transgenic lines were obtained. β-Glucronidase staining was performed according to the published method (Jefferson et al., 1987).

Differential Gene Expression Analysis

Seeds of the WT and *roses1* mutant were grown in an artificial climate incubator under 12 h light (300 μmol m^{-2} s^{-1}) at 24°C and 12 h dark at 18°C with 60% relative humidity for 7, 14, and 21 d, respectively. Seedling leaves were harvested and frozen immediately in liquid nitrogen. Equal amounts of harvested samples were mixed for respective genotypes and subjected to total RNA isolation and RNA sequencing experiments. Three biological replications were performed.

Total RNAs were extracted from the samples by using Trizol reagent, treated with DNase I and further purified with an RNA clean kit (Promega). RNA quality and purity were assessed with an Agilent 2100 Bioanalyzer RNA Nanochip (Agilent) and a Nano Drop ND-1000 Spectrophotometer, respectively. Sequence tag libraries were constructed and sequenced using an Illumina HiSeq 2000 sequencing platform following the manufacturer's instructions. Raw reads have been deposited in the NCBI sequence read archive under the accession number PRJNA339657. More than 10 million clean reads were obtained in each sample. All clean reads were aligned to the rice reference sequence using Tophat2 (Trapnell et al., 2009), and no more than three nucleotide mismatch was allowed. The number of clean reads for each mapped gene was calculated and then normalized into reads per kilobase of exon model per million mapped reads. Differentially expressed genes (DEGs) were defined with a relative change threshold of twofold (P value < 0.01, false discovery rate < 0.01).

RESULTS

Distinct Reduction of Organ Size Resulting from Decreased Cell Number and Reduced Cell Size in *roses1*

About 30,000 seeds derived from *indica* cultivar Fuhui9802 were treated with mutagen EMS. One mutant showing distinct reduction of organ size with precocious leaf senescence was obtained and designated as *reduced organ size with early senescence 1* (*roses1*). Obviously, the agronomic traits of the *roses1* mutant were found inferior to those of the WT Fuhui9802 plants. The means of plant height, effective panicle number per plant, panicle length, grain number per panicle, frequency of seed set, and 1000-grain weight of the *roses1* mutant were 80.68, 70.37, 88.59, 80.82, 74.04, and 84.23% those of the WT plants (Table 1). In particular, the reduced grain number per panicle of *roses1* was caused by highly significant reductions in both primary branch number and secondary branch number, and the reduced 1000-grain weight of *roses1* resulted from reduction in the size of its seeds. Thus, the morphological alterations caused by the *roses1* mutation had significant impact on agronomic traits of the rice plant.

We compared the altered morphology of the *roses1* mutant with the WT plant. The overall growth and development of the *roses1* mutant plant were significantly inhibited (Fig. 1a–1c, Supplemental Table S3). Distinct reduction in plant height and sizes of root, culm, leaf, panicle, spikelet, and floral organs was observed in the *roses1* mutant plant (Fig. 1a–1m, Supplemental Table S3). The *roses1* mutation leads to a decreased number of roots, tillers, primary and secondary panicle branching, grains per panicle, and vascular bundles in stems and leaves that were visualized (Fig. 1, Supplemental Table S3). The distinct reduction of plant size in *roses1* apparently results from the shortened internodes (Fig. 1d, Supplemental Table S3) and reduced size of culm diameter (Fig. 1e, Supplemental Table S3). Thus, we further investigated relative cell number and cell size of the stem internodes using microscopy section analysis. Longitudinally, the second internode to the top in *roses1* was characterized with a much lower cell number (39.2%) and slightly smaller cell size (9.8%) than the WT (Fig. 1f, Supplemental Table S3). Transversely, the huge difference in culm diameter between *roses1* and WT likewise resulted from drastic reduction of cell number (19.0%) and slightly reduced cell size (11.1%) in *roses1* (Fig. 1g and 1h). Thirty-nine or thirty-two vascular bundles were observed in culms of WT or *roses1*, respectively (Fig. 1g, Supplemental Table S3). Similarly, a decrease in *roses1* mutant leaf size with 11 veins was observed as compared with the 14 veins of WT leaf blade (Fig. 1i–1k, Supplemental Table S3). Moreover, significant reduction in tiller number, effective panicle number per plant, pollen fertility, seed-setting rate, grain size and weight, and embryo size was detected in *roses1* mutant (Fig. 1b, 1c, 1n–1r; Supplemental Table S3).

Table 1. Important agronomic traits of the wild-type (WT) Fuhui9802 and a *reduced organ size with early senescence* (*roses1*) mutant.

Genotype	Plant height	Effective panicle no. per plant	Panicle length	Grain no. per panicle	Primary branch no.	Secondary branch no.	Seed set	1000-grain weight	Seed length	Seed width
	cm		cm				%	g	mm	
WT	118.5 ± 6.6	10.8 ± 1.3	29.8 ± 2.3	172.6 ± 9.8	13.1 ± 1.5	20.4 ± 2.1	88.6 ± 7.3	26.0 ± 1.0	9.4 ± 0.2	2.9 ± 0.1
roses1	95.6 ± 4.3**	7.6 ± 1.0**	26.4 ± 1.0**	139.5 ± 7.7**	10.2 ± 1.8**	15.9 ± 1.8**	65.6 ± 4.5**	21.9 ± 0.9**	9.1 ± 0.3*	2.8 ± 0.1

*,** Significant at the 0.05 and 0.01 probability levels, respectively.-

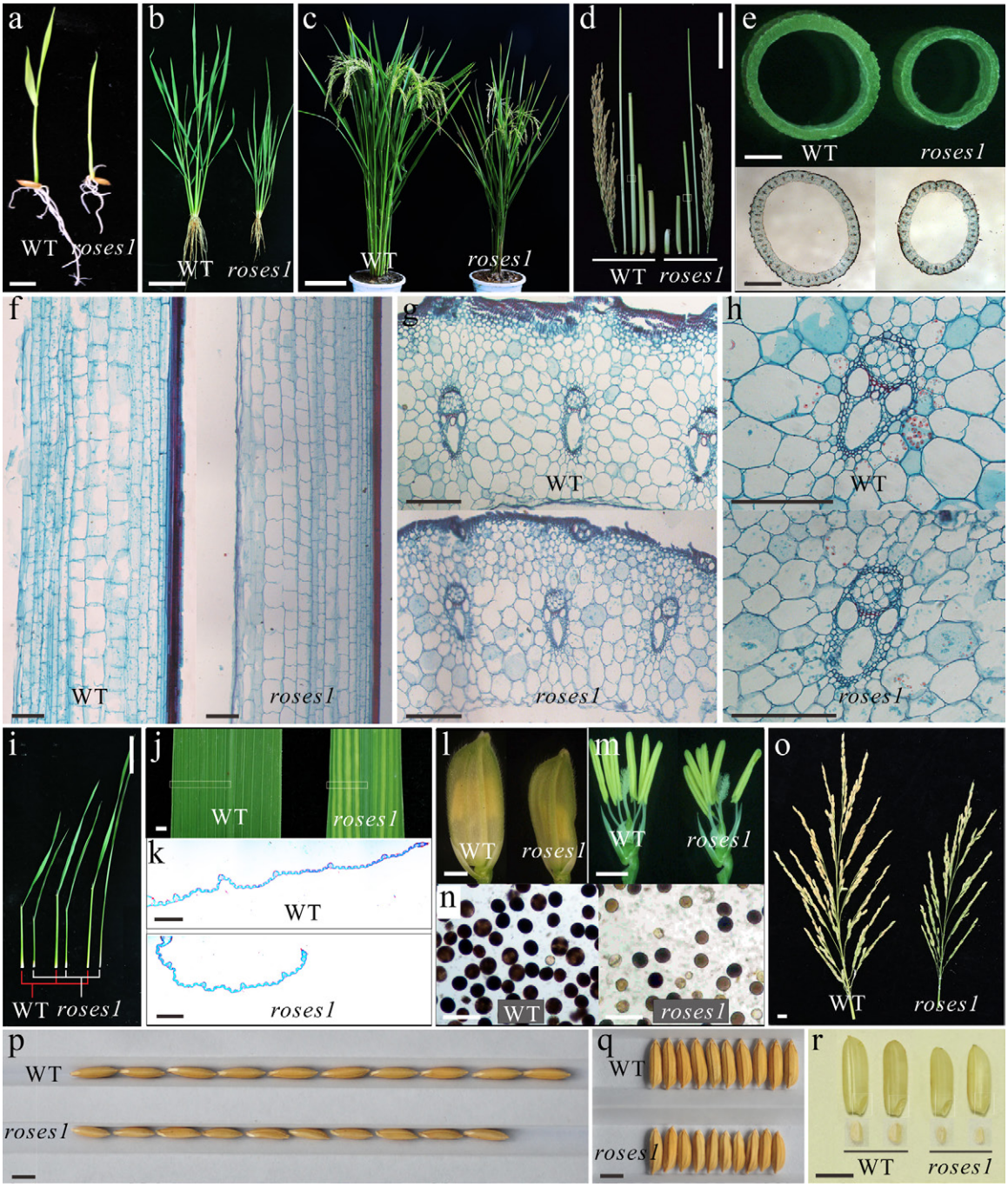

Fig. 1. Phenotypic characterization of the *roses1* mutant and its wild-type (WT) Fuhui9802 plant. (a) 10-d-old plants, bar = 1 cm. (b) 60-d-old plants, bar = 5 cm. (c) Mature plants, bar = 10 cm. (d) The separated internodes and the panicles of WT and *roses1*, bar = 10 cm. (e) Transverse section of the middle part of the second internode from the top in the WT and *roses1*, bar = 0.2 cm. (f) Longitudinal sections of culms, bars = 20 μm. (g, h) Cross-sections of culms of WT and *roses1* plants, bars = 50 μm. (i) Length comparison of first to third leaves between the WT and *roses1* mutant at heading stage, bars = 10 cm. (j, k) Transverse sections of the 12th leaf blade of WT and *roses1* plants, bars = 2 mm. (l) Spikelets of WT and *roses1*, bars = 2 mm. (m) Flowers of WT and *roses1*, bars = 2 mm. (n) Pollen grains sampled from spikelets just before flowering and stained with iodine and potassium iodide solution, bars = 0.3 mm. (o) Panicles of the WT and *roses1* plants, bar = 1 cm. (p, q) Comparison of length and width of grains and seeds between the WT and *roses1* mutant, bar = 0.5 cm. (r)Comparison of the unhusked grains and the separated embryos between the WT and *roses1* mutant, bar = 0.5 cm.

roses1 Displays Premature Senescence with Underdeveloped Chloroplast and Reduced Content of Photosynthesis Pigment

Remarkably, the *roses1* leaves began to develop longitudinally whitening stripes in parallel to the leaf veins at the tillering stage, and the stripes became pale brown at the heading stage. To determine whether the color change in *roses1* leaves could be due to pigmentation alteration, the contents of photosynthetic pigments were measured in both WT and *roses1* leaves at three different developmental stages.

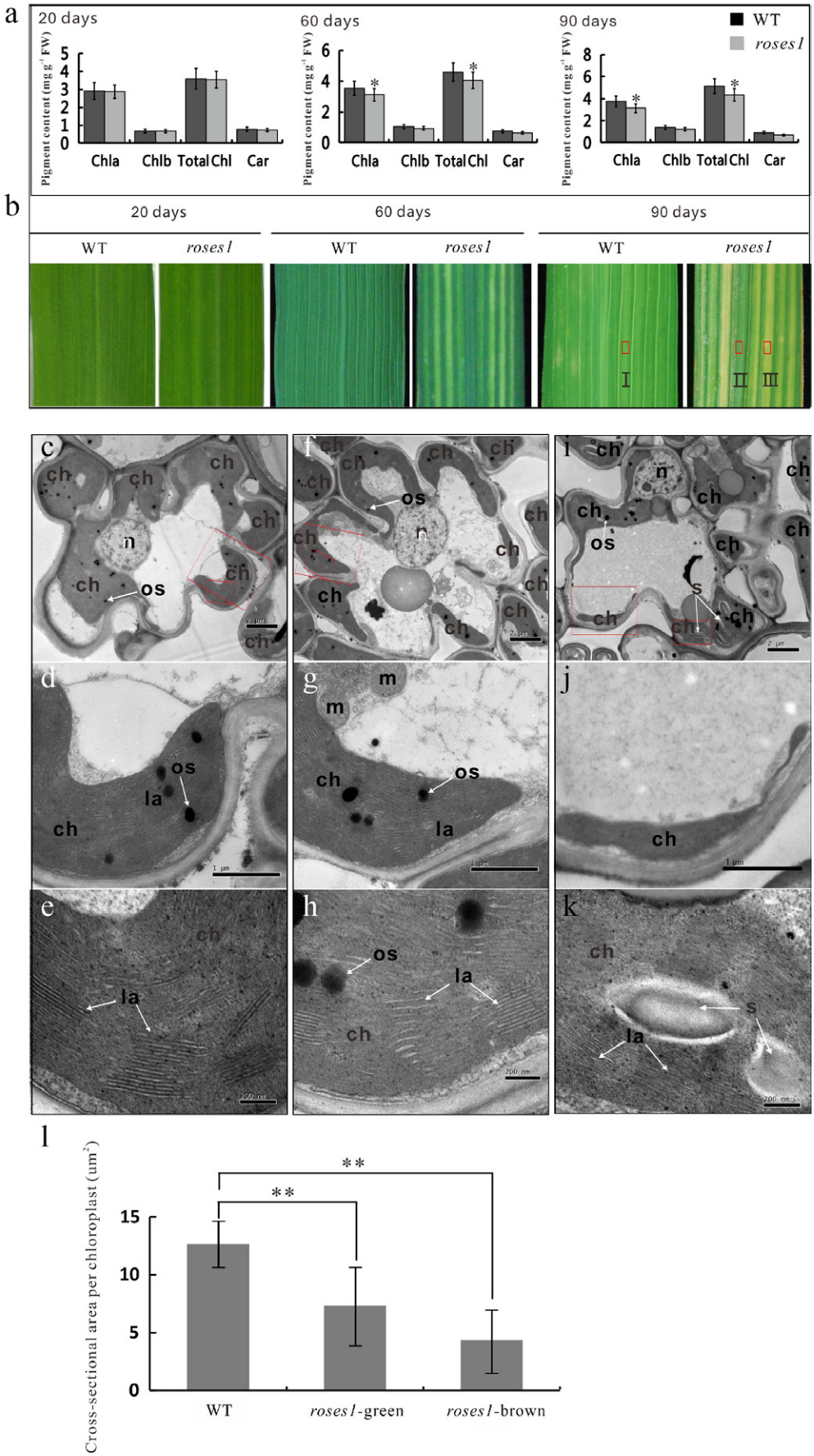

Fig. 2. Phenotypic comparisons in terms of photosynthetic pigments and chloroplast development between the wild-type (WT) and *roses1*. (a) The contents of photosynthetic pigments in WT and *roses1* leaves at different developmental stages (n = 9). (b) The pale brown stripes developed in *roses1* leaf at tillering (60-d-old) and heading (90-d-old) stages. (c–k) Sections viewed by transmission electron microscopy showing the structure of mesophyll cells and their chloroplasts enclosed. (c–e) The middle part of the WT flag leaf. (f–h) Green portion of pale brown striped flag leaf from *roses1*. (i–k) Brown portion of the *roses1* flag leaf. (l) The comparison of average chloroplast compartment size. Chla, chlorophyll a; Chlb, chlorophyll b; Total Chl, total chlorophyll; Car, carotenoid; n, nucleus; ch, chloroplast; la, lamella; s, starch grain; os, osmiophilic body; m, mitochondrion. * Significant at the 0.05 probability level, ** significant at the 0.01 probability level.

The results showed that, at the seedling stage (20 d old), no significant difference in pigment content was observed between WT and *roses1* leaves (Fig. 2a and 2b). By contrast, the total pigment content was significantly lower in *roses1* than in the WT at the tillering stage (60 d old). The chlorophyll a content in the *roses1* leaf was 88.7% of that measured in WT, whereas the total chlorophyll content in the *roses1* leaf was 89.8% of that in WT. At heading stage (90-d-old), the total pigment content was also significantly lower in *roses1* than in WT. The content of chlorophyll a in the *roses1* leaf was reduced to 87.7% of that measured in WT, whereas the total chlorophyll content in *roses1* leaf was reduced to 87.9% of that in WT. No significant change in chlorophyll b or carotenoid content was detected (Fig. 2a)

To determine whether *roses1* mutation causes any developmental defects in leaves, TEM was employed. From the middle part of the flag leaf at the heading stage (90 d old), green or pale brown portions of the *roses1* leaf and the corresponding regions of WT were sampled separately (Fig. 2b). Although normally arranged grana and lamellae were observed in all three samples, the chloroplast compartment size was significantly reduced in the *roses1* cells from either green or pale brown portions compared with that of WT (Fig. 2c–2l), in which the reduction was greater in *roses1* cells from the pale brown portion than from the green portion, indicating that the development of chloroplast was severely retarded in the *roses1* mutant.

To assess changes in photosynthesis in WT Fuhui9802 and *roses1* plants at the heading stage, photosynthetic parameters of the *roses1* and WT plants grown in the field were determined using a LI-6400 photosynthesis meter. The results showed that the photosynthetic rate was 6.67 and 13.34 μmol m^{-2} s^{-1} in *roses1* and WT plants, respectively (Supplemental Table S4). The stomatal conductance of *roses1* leaves was 0.11 mol H_2O m^{-2} s^{-1}, which was only 28.9% of the stomatal conductance of WT leaves. The transpiration rate of *roses1* leaves was 59.8% lower than that of the WT leaves (Supplemental Table S4). However, no significant difference of intercellular CO_2 concentration was found between the *roses1* and WT plants (Supplemental Table S4). Nevertheless, the photosynthesis rate, stomatal conductance, and transpiration rate were significantly lower in the *roses1* leaves than in the WT leaves, suggesting that the *roses1* mutation plays a significant role in photosynthesis in rice.

Leaf Rolls in *roses1* Probably Due to Elevated Stomatal Density

Interestingly, transverse leaf rolling occurring in the *roses1* was easily viewed in field-grown plants, and extremely rolled leaves occurred in the 60-d-old *roses1* mutant plants (Fig. 3a–3c). At this time, the LRI of *roses1* reached ~71.8%, whereas 0.8% of LRI was detected in WT leaves (Fig. 3d). Significantly, transverse sections showed bulliform cells in the rolled *roses1* leaves that were atrophied and had size reduced by 31.2% (Fig. 3e and 3f, Supplemental Table S3), suggesting a severe water loss imposed by excessive transpiration in *roses1* leaves.

To determine if transpiration is related to the *roses1* leaf phenotype, the LRI was measured in response to an increment of environmental temperatures. The WT and *roses1* plants were grown in growth chamber at temperatures of 24, 28, 32, and 36°C, respectively. As shown in Fig. 3g to 3i, the WT plants constantly exhibited outspread leaves, whereas gradually increased LRI was detected in *roses1* leaves with the increased temperatures, eventually approaching a cylinder shape at 36°C. Thus, the *roses1* mutation leads to an increased LRI in response to elevation of environmental temperatures, strongly suggesting that increased water release occurred through the *roses1* mutant leaves via enhanced stomatal transpiration.

To characterize the stomatal development and movement in the *roses1* mutants, we analyzed the effects of the *roses1* mutation on stomatal density and aperture. Leaf surfaces were processed for SEM observation to determine the numbers and distribution of stomata. As shown in Fig. 4a and 4b, compared with the WT, there was an increased density of stomata developed on both the abaxial and adaxial surfaces of the *roses1* leaf, and the average number of stomata per square millimeter of leaf surface increased by 18.8 and 22.0% on the abaxial and adaxial surfaces, respectively (Fig. 4c). Meanwhile, the length of stomatal cell in the *roses1* mutant was recorded as 88.3 or 90.1% as that of WT (Fig. 4d, Supplemental Table S3).

We next examined water loss in *roses1* leaves. Detached intact leaves from 60-d-old plants were maintained at room temperature, and the fresh weight was measured every half hour for a 2.5-h time period. The *roses1* leaves showed a much greater rate of water loss than the WT leaves (Fig. 4e, Supplemental Table S5). As the stomata could be classified as the completely open, partially open, or completely closed, the stomatal aperture in WT and *roses1* leaves was accordingly determined under constant temperatures of 22, 30, or 38°C for 2 h, respectively (Fig. 4f). Under 22°C, compared with 14.6% completely closed and 43.1% completely open stomata in WT leaves, 15.9% completely closed and 45.2% completely open stomata were observed in *roses1* leaves. Under 30°C, compared with 35.1% completely closed and 19.8% completely open stomata in WT leaves, 33.2% completely closed and 25.4% completely open stomata were observed in *roses1* leaves. Under 38°C, compared with 72.9% completely closed and 1.2% completely open stomata in WT leaves, 68.9% completely closed and 4.3% completely open stomata were observed in *roses1* leaves. These results indicate that, under various temperature conditions, stomatal aperture opening in the *roses1* mutant was greater than in the WT.

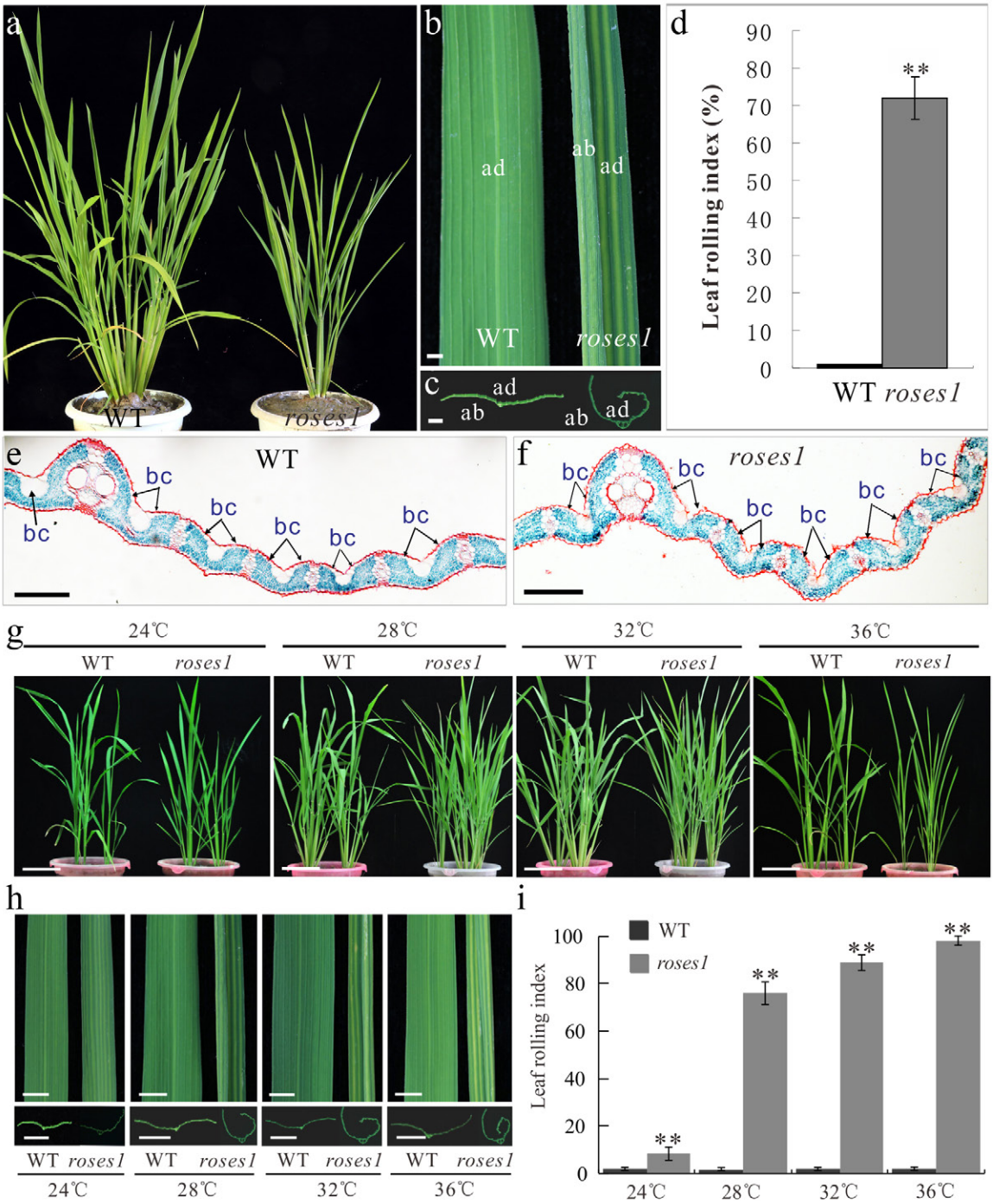

Fig. 3. Phenotypic comparison of leaf rolling between the wild-type (WT) and *roses1* plants. (a, f) Increased leaf rolling caused by *roses1* mutation observed in natural condition. (a) Morphology of the WT and *roses1* plants grown in pots. (b) Enlarged views of the WT and *roses1* leaves, bars = 2 mm. (c) Cross-section of the WT and *roses1* leaves, bars = 2 mm. (d) Leaf rolling index of the WT and *roses1* plants (n = 10). (e, f) Cross-sections of the mature 12th leaves from the WT and *roses1* plants, bars = 50 μm. (g–i) Comparison of leaf rolling index alteration in response to artificial growth conditions between WT and *roses1*. (g) Differential leaf rolling index occurring in WT and *roses1* plants grown under four different constant temperatures (24, 28, 32, and 36°C, respectively), bars = 10 cm. (h) Enlarged views of the WT and *roses1* leaves, as well as their corresponding cross-section, bars = 1 cm. (i) Leaf rolling index of the WT and *roses1* plants under the four different temperatures (n = 5). bc, bulliform cell; ab, abaxial; ad, adaxial. ** Significant at the 0.01 probability level.

ROSES1 Encodes a Nucleus-Localized Homeobox Domain Protein

We next sought to clone the *roses1* mutant gene by map-based cloning. To this end, we developed two F_2 populations by crossing a *roses1* mutant to two *indica* cultivars, ZhongjiuB and Q4B, respectively. All of the F_1 plants displayed the WT phenotype. In both F_2 populations, the WT and mutant phenotypes showed a typical 3:1 segregating ratio (Supplemental Table S6). This result suggested

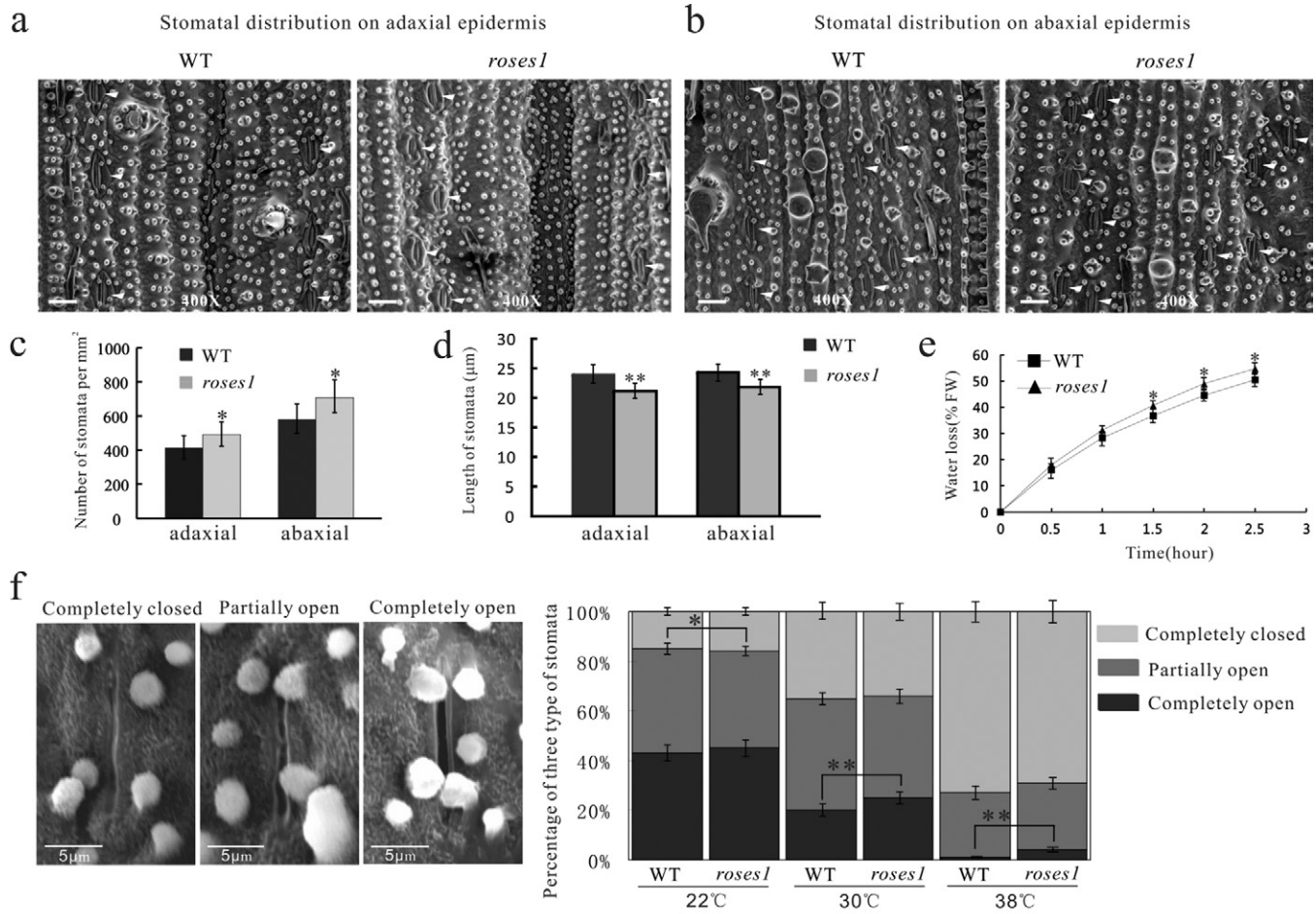

Fig. 4. Phenotypic comparisons of leaf stomatal parameters and water loss rate between the wild-type (WT) and *roses1* plants. Flag leaves were sampled. Stomatal analysis was performed using a scanning electron microscope. Water loss rate was calculated by measuring leaf weights at sets of time intervals. (a, b) Scanning electron micrograph images (400×) of the adaxial and abaxial leaf epidermis, where stomata is marked by triangular arrowheads, bars = 20 μm. (c) Average stomata numbers per square millimeter calculated from 10 sampled leaves, indicating the differential stomata densities. (d) Comparison of the stomata length between WT and *roses1* plants (n = 20). (e) Comparison of water loss rate between the WT and *roses1* plants. (f) Scanning electron microscopy images of three different opening levels (completely closed, partially open, and completely open) of rice stomata (upper part) under constant 22, 30, or 38°C for 2 h, respectively. The stomata percentage at three levels in WT and *roses1* was measured (n = 150) (lower part). Bars = 5 μm. * Significant at the 0.05 probability level, ** significant at the 0.01 probability level.

that the *roses1* mutation was controlled by a single recessive nuclear gene.

We used 1595 individual F_2 plants with reduced organ size and green-brown striped early senescence leaves, derived from the cross between ZhongjiuB and *roses1*, for molecular mapping. Equal amounts of leaf tissue from each of 10 WT plants and 10 *roses1* plants were collected for DNA extraction to form a WT DNA pool and a mutant DNA pool, respectively. A total of 480 SSR markers evenly covering the 12 chromosomes were applied for polymorphism analysis between the two parents, ZhongjiuB and *roses1*. Of these markers, 32 pairs of primers showed polymorphism and were further used to screen the two DNA pools. The polymorphic markers RM135 and RM1230 were used to analyze 15 normal F_2 individuals and 15 mutant F_2 individuals to confirm linkage between the primers and the mutation. In addition, 12 SSR markers were designed to refine the chromosomal location of the gene. Using the 312 F_2 individuals showing the *roses1* mutant phenotype, *ROSES1* was mapped preliminarily to chromosome 3 between the primers RM168 and RM1230, with genetic distances of 6.73 and 15.54 cM, respectively (Fig. 5a). To further narrow down the primary mapped region, an additional 20 SSR markers were designed for a population of 1595 mutant F_2 individuals. Four markers, RM15861, RM15864, RM15872, and RM15883, revealed polymorphism between the two parents, with 19, 3, 12, and 26 recombinants, respectively. These results showed that *ROSES1* was located between the SSR markers RM15864 and RM15872, in which the physical distance was ~42.4 kb according to the the reference Nipponbare genome sequence derived from the Gramene database (McCouch et al., 2002; Ware et al., 2002) (Fig. 5a).

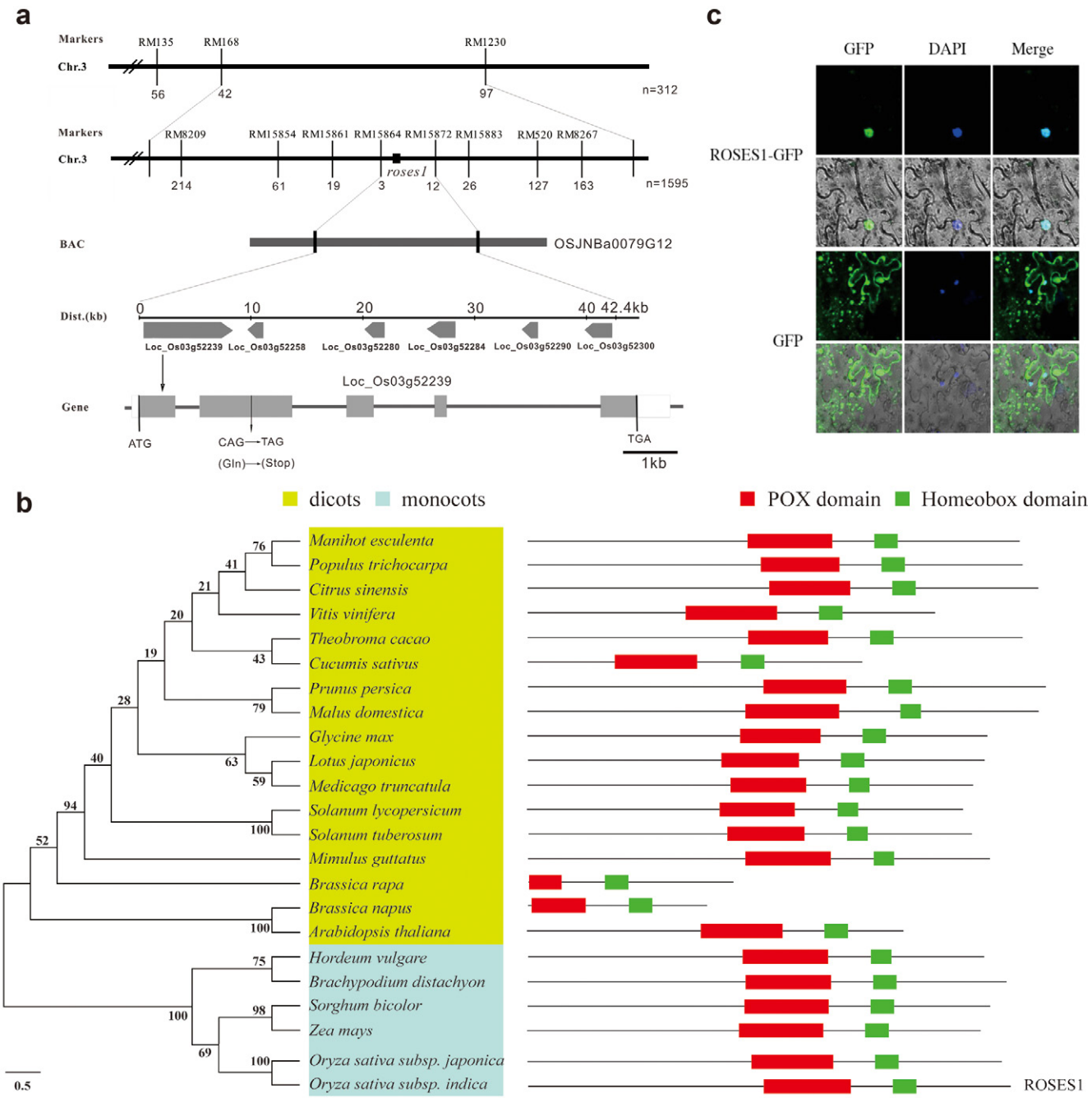

Fig. 5. Map-based cloning, subcellular localization, and phylogenetic analysis of the *ROSES1*. (a) Fine mapping of the *roses1* locus. The relative positions of bacterial artificial chromosome clones (BACs) are shown. The site of *roses1* mutation is shown. Sequence alignments indicating a C to T mutation in a CAG codon creates a TAG premature termination codon in the second exon of the predicted open reading frame coding for a homeobox transcription factor (TF) protein. (b) Phylogenetic analysis of the ROSES1 homologs derived from 23 species, and two major clades could be classified (left). The deduced homeobox domain and peroxidase (POX) domain are indicated (right). (c) Analysis of the subcellular localization of the ROSES1 protein. *p35S::ROSES1-GFP* and *p35S::GFP* constructs were introduced separately into tobacco epidermal cells by infiltration, and the expressed signal was observed under a confocal microscope (FV1000, Olympus).

Within this 42.4-kb region, there were six predicted open reading frames according to the genomic sequence of Nipponbare (McCouch et al., 2002; Ware et al., 2002). To determine the mutation site, the genomic region containing the six putative coding sequences was isolated from both the *roses1* mutant and the WT Fuhui9802 (Supplemental Table S1). Sequence alignments revealed that, in the *roses1* mutant, a C to T mutation in a CAG codon created a TAG premature termination codon in the second exon of the predicted gene coding for a homeobox TF protein. No other base changes in the six predicted genes were found between the *roses1* mutant and the WT plants (Fig. 5a). In addition, we have conducted the real-time PCR to determine the expression of these six candidate genes in both WT and *roses1* mutant plants. Our results indicate there is no significant difference of the expression of these six

candidate genes between the WT and the *roses1* mutant (Supplemental Fig. S1). These results also suggest that C to T mutation in the *ROSES1* gene has no effect on the transcripts of any of the six candidate genes.

The putative *ROSES1* gene (BGIOSGA013510 in *O. sativa* ssp. *indica* and LOC_Os03g52239 in *O. sativa* ssp. *japonica*) encodes a protein containing 779 amino acids. The predicted protein belongs to the BEL1-like homeobox subfamily and possesses two functional domains, the DNA binding homeobox domain and an unknown-function POX domain that is found exclusively in plants associated with the homeobox domain protein (Doerks et al., 2002). The phylogenetic analysis suggests that these proteins are highly conserved during evolution and that the phylogenetic tree could be subdivided into two major clades, the monocot clade and dicot clade (Fig. 5b). According to the domain identification, the homeobox domain and the POX domain are present in all the ROSES1 homologs from both monocot and dicot clades, suggesting that the ROSES1 protein might appear before the divergence of monocots and dicots (Fig. 5b). Since TFs are generally localized in the nucleus, we verified the subcellular localization of the ROSES1 protein by confocal microscopy analysis of the ROSES1-GFP fusion protein. As shown in Fig. 5c, the ROSES1-GFP signal was visualized in the nucleus, whereas GFP alone was detected throughout the cells. These results suggest that ROSES1 is a nuclear protein, which is consistent with the notion that TFs typically function within the nucleus to regulate gene expression.

Expression Pattern of the *roses1* Gene

To study the expression pattern of *ROSES1*, the GUS reporter construct (*pROSES1::GUS*) driven by the *ROSES1* promoter was generated and transformed into the WT Fuhui9802. Staining of transgenic plants demonstrated that the GUS signal was detected at the root meristem and elongation zone, shoot meristemoids, culm nodes, culm intercalary meristem, leaf, inflorescence branch and stem, spikelet, and developing caryopsis and embryo (Fig. 6).

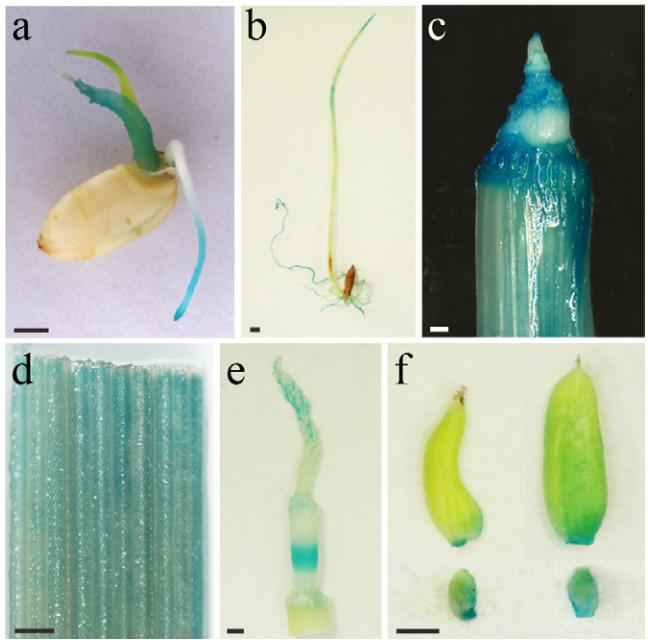

Fig. 6. Expression pattern of ROSES1. (a–f) Expression signal showing in (a, b) seedling root and leaf, (c) shoot, (d) developing leaf at tillering stage, (e) developing internode and panicle branch, and (f) developing caryopsis and embryo, bars = 0.2 cm.

Transcriptomic Analysis

To explore the gene expression characteristics and molecular mechanisms underlying the *roses1* mutant rice, differential gene expression (DGE) analysis was performed using Illumina technique to investigate DEGs between the WT and mutant leaf samples grown under 24°C at three developmental stages (7-, 14-, and 21-d-old seedling), as well as leaf samples grown under 32°C at one stage (21-d-old seedlings). At 24°C, a total of 2166 genes were identified as DEGs, 1171 (54%) of which were upregulated and 995 (46%) of which were downregulated by at least twofold in the mutant ($roses1_{24}$) compared with WT (WT_{24}) samples (Supplemental Table S7). At 32°C, a total of 1088 genes were detected with greater than twofold different expression, of which 482 (44%) were upregulated and 606 (56%) were downregulated in the mutant ($roses1_{32}$) compared with WT (WT_{32}) samples (Supplemental Table S8). Among these DEGs, several rice genes orthologous to well-characterized organ- and cell-size-enlarged genes were found downregulated in the *roses1* mutant, such as *SAUR* (Spartz et al., 2012), *NGA* (Ballester et al., 2015), *CAX1* (Conn et al., 2011), *GPT2* (Van Dingenen et al., 2016), and *SNARE* (Löfke et al., 2015). In comparison, *RALF* (Bergonci et al., 2014) and *RPT2a* (Kurepa et al., 2009), reported to negatively control organ growth, were upregulated in the *roses1* mutant. These results suggested that loss-of-function mutation of *roses1* reduced the transcript levels of some key positive regulators and elevated the transcript levels of some negative regulators, thus reducing the organ size of root, leaf, stem, inflorescence, spikelet, and florets. We also identified several DEGs that were supposed to regulate stomata development and density in leaves, such as *PLD* (Uraji et al., 2012), *RD20* (Aubert et al., 2010), *MYB44* (Jung et al., 2008), and *RLKs* (Shpak et al., 2005).

We further inspected the functional classification of the above DEGs over the gene ontology (GO) annotation for biological processes and molecular functions (Ashburner et al., 2000). Generally, proteins in each DEG possess a similar distribution pattern across the GO slim categories (cut-down versions of the GO slim categories). A number of regulatory proteins and functional proteins were identified (Fig. 7). Among them, TFs and

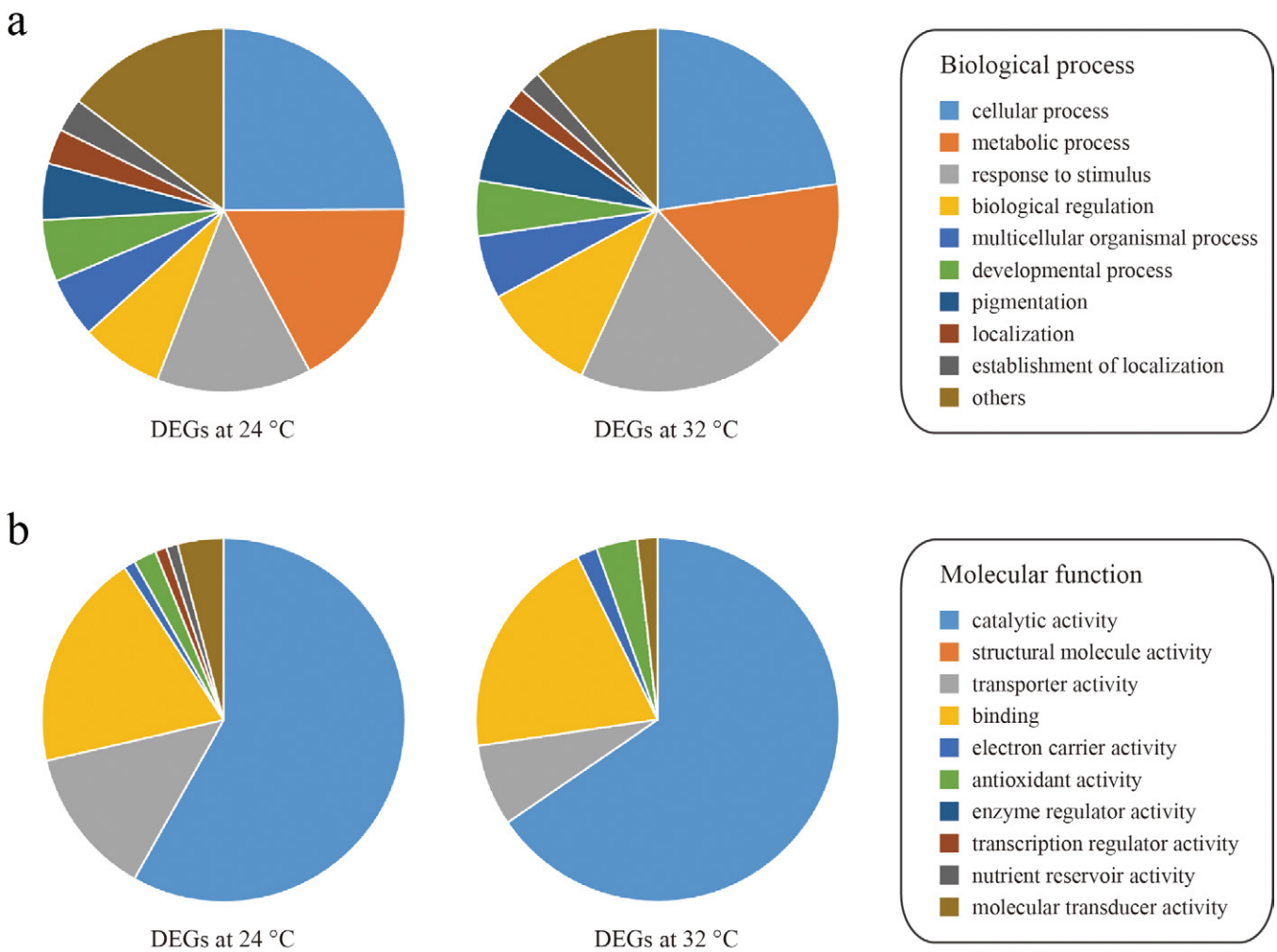

Fig. 7. The gene ontology annotation of enriched proteins in differentially expressed genes (DEGs) at 24 and 32°C, respectively. (a) The biological process category. (b) The molecular function category.

protein kinases could be involved in signal transduction, whereas the small heat shock proteins often play protective roles in response to various stresses, and transporters could regulate osmotic pressure by the movement of water across membranes. Using the proteins in the entire rice proteome as background for significance testing (hypergometric test), we found that DEGs between *roses1*$_{24}$ and WT$_{24}$ were significantly enriched in starch biosynthetic process (GO: 0019252), stomatal complex morphogenesis (GO: 0010103), chloroplast relocation (GO: 0009902) and photosystem II assembly (GO: 0010207) (Supplemental Table S9). The most enriched gene categories in DEGs between *roses1*$_{32}$ and WT$_{32}$ were related to stomatal complex morphogenesis (GO: 0010103), response to growth hormone (GO: 0060416), electron transport chain (GO: 0022900) and de-etiolation (GO: 0009704) (Supplemental Table S10). These results implied that ROSES1 protein had a global impact on the gene expression profile during rice development, consistent with the mutant phenotypes of reduced plant size and early leaf senescence with underdeveloped chloroplast and photosystems.

To determine whether the mutation of *ROSES1* affected the messenger RNA expression of some candidate downstream genes in regulating cell enlargement and stomata development, quantitative real-time PCR analysis was performed on WT and *roses1* mutant leaves over the same period of development at the seedling stage. The primers used for these analyses are listed in Supplemental Table S1. Quantitative real-time PCR results showed that the expression level of five positive regulators of cell enlargement, such as rice homologs of *SAUR*, *NGA*, *CAX1*, *GPT2*, and *SNARE*, was reduced to different extents in *roses1* mutant compared with that of WT (Fig. 8); however, the expression level of negative regulators of cell enlargement such as *RALF* and *RPT2a* were increased. Additionally, increased expression level of genes involved in regulating stomata development and density in leaves such as *PLD*, *RD20*, *RLKs*, and *MYB44* were detected in the *roses1* mutant (Fig. 8). These results were consistent with those findings that have been investigated by analyzing DEGs between the WT Fuhui9802 and *roses1* plants.

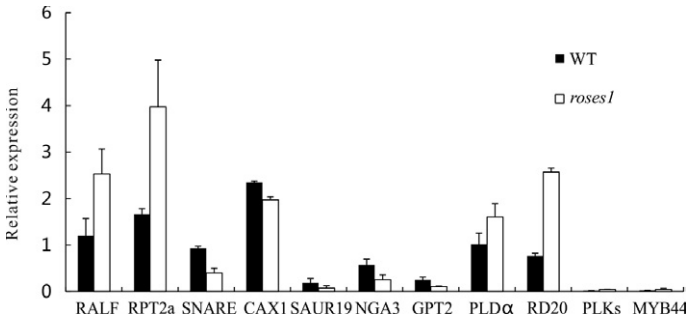

Fig. 8. Expression analysis of genes associated with organ- and cell-size-enlarged and stomata development in the *roses1* mutant and wild-type (WT).

DISCUSSION

In this work, we have isolated and characterized the rice *roses1* mutant displaying distinctly reduced organ size and precocious leaf senescence. Phenotypic analyses of the *roses1* mutant demonstrated that the drastic reduction in organ size was attributed to decreased cell number and cell size, whereas early leaf senescence probably resulted from increased stomatal density. Fine mapping showed that *ROSES1* encodes a homeobox protein ortholog containing a homeobox domain and a plant-specific unknown-function POX domain. As a homeobox TF, its nuclear localization was confirmed by visualizing the expression signal of the ROSES1-GFP fusion protein in nucleus. Meanwhile, *ROSES1* expression pattern was investigated using GUS reporter gene driven by the *ROSES1* promoter, and the GUS staining signal was detected mainly at root or shoot meristemoids, intercalary meristemoids, and vascular tissues.

ROSES1 is a General Homeobox Regulator Required for Both Primary Meristem Initiation during Embryogenesis and Secondary Organ Primordia Development

Our investigations suggest that *roses1* mutation gives rise to sharp decline of the numbers of axillary organs and tissues, including lateral roots, tillers (shoot branches), panicle branches, spikelets, culm vascular bundles, and leaf veins. Longitudinally, reduction of the mutant plant height is apparently due to the shortened internodes with a reduced cell number, but without altering the number of nodes or internodes. We postulated that these tremendous changes were most likely due to the reduced primary root or shoot meristem size during *roses1* embryogenesis, evidenced by the reduced grain size and embryo size.

Extensive studies on the shoot apical meristem and root apical meristem that generate all above- and belowground organs and tissues, respectively, have unraveled that highly similar organizational and genetic programs underlie both stem-cell systems, with many of the individual genes being encoded by closely related, tissue-specific homologs (Galli and Gallavotti, 2016). In *A. thaliana*, meristem maintenance is regulated by the negative feedback loop of *WUSCHEL-CLAVATA* (*WUS-CLV*) that was established as being essential for regulating the size of shoot meristems by maintaining a delicate balance between stem cell proliferation and cell recruitment for the differentiation of lateral primordia (Mayer et al., 1998; Fletcher et al., 1999; Brand et al., 2000; Schoof et al., 2000; Reddy and Meyerowitz, 2005; Barton, 2010; Ha et al., 2010; Yadav et al., 2010; Aichinger et al., 2012). The regulator WUS is the founding member of the *WUSCHEL*-related homeobox (*WOX*) plant-specific subfamily of homeobox transcriptional regulators that function in multiple developmental pathways (Mayer et al., 1998; van der Graaff et al., 2009). The rice *WUS* ortholog is required specifically for initiating the premeristem of tillers (shoot branches) (Tanaka et al., 2015). Meanwhile, the rice *WOX* genes were shown to be specifically involved in maintenance of the root apical meristem and crown root development (Kamiya et al., 2003; Zhao et al., 2009). Likewise, the rice *ORYZA SATIVA HOMEOBOX1* (*OSH1*), a class 1 *knotted-like homeobox* (*KNOX*) gene (Long et al., 1996), was demonstrated to specifically promote the undifferentiated state of the shoot meristem (Sato et al., 1996; Tsuda et al., 2011). In the rice *osh1* mutant, the shoot apical meristem can be formed but not maintained after germination. The shoot apical meristem is not established in the double mutant of *osh1* and *d6* (coding for the related homeobox protein OSH15), indicating that both genes are probably required for formation or maintenance of the shoot apical meristem during embryogenesis in rice (Tsuda et al., 2011). Our work found that the ROSES1 protein belongs to the BEL1-like homeobox subfamily and possesses two functional domains, the DNA-binding homeobox domain and a plant-specific unknown-function POX domain (Doerks et al., 2002). Distinct from the rice *WUS* ortholog or other homeobox genes that are required specifically for either shoot or root meristem initiation or axillary organ primordial formation, ROSES1 seems to be a general regulator and is required for both primary meristem initiation during embryogenesis and secondary meristem origination of all axillary organs and tissues, such as lateral roots, tillers, panicle branches, spikelet primordia, and vascular bundles that either radially surround the culm or flank the main vein of the leaf blade. How the *ROSES1* acts and coordinates with *WUS* or other homeobox genes to regulate meristem maintenance require further investigation.

ROSES1 Affects Plant Size through Regulating Both Cell Proliferation and Cell Expansion

The mechanism of organ size control is a fundamental question in developmental biology. The plant organ growth is determined by cell number, cell size, or both that result from coordinated regulation of cell proliferation

and cell expansion during organogenesis (Mizukami, 2001; Sugimoto-Shirasu and Roberts, 2003). In the present work, we demonstrate that ROSES1 is a master player of organ size control by influencing both cell proliferation and cell expansion. We believe that, comparing the WT and *roses1* mutant, the altered stem cell number existing in the primary apical meristems of embryo gives rise to not only the differential cell number in apical organ primordia for organs like internodes or inflorescence and panicle, but also the altered architecture or number of axillary organ primordia, such as lateral roots, tillers, culm vascular bundles, leaf veins, and panicle branches. Apparently, a large part of the distinct reduction of *roses1* culm diameter and leaf blade width could be attributed to the reduced vascular bundle number and the total cell number enclosed in the organs. Meanwhile, a decreased size was detected in the culm cells, leaf stomatal cells, leaf bulliform cells, and pollen cells of *roses1*.

To explore the expression regulatory network by ROSES1, we conducted DGE analysis using the Illumina technique. A large number of DEGs between the WT and *roses1* mutant were identified. Among these DEGs, several rice orthologs of well-characterized positive regulators of cell enlargement were found downregulated in the *roses1* mutant and could be the direct targets of ROSES1, such as SAUR (Spartz et al., 2012), NGA (Ballester et al., 2015), CAX1 (Conn et al., 2011), and SNARE (Löfke et al., 2015). Consistently, rice genes homologous to *RALF* (Bergonci et al., 2014) and *RPT2a* (Kurepa et al., 2009), characterized to negatively control cell expansion, were upregulated in the *roses1* mutant. The *SAUR* genes comprise the largest family of auxin responsive genes and are positively involved in regulating cell expansion (Spartz et al., 2012). The SAUR inhibition of PP2C-D phosphatases activates plasma membrane H^+-ATPases to promote cell expansion (Spartz et al., 2014). The *NGA* genes are TFs that influence cell expansion by associating auxin signaling (Trigueros et al., 2009; Martinez-Fernandez et al., 2014). CAX1 (Ca^{2+}/H^+-antiporter), a tonoplast-localized Ca^{2+} transporter, was shown as a key regulator of apoplastic [Ca^{2+}] through compartmentation into mesophyll vacuoles, a mechanism essential for optimal plant function and productivity (Conn et al., 2011). The SNAREs are essential for eukaryotic vesicle trafficking and homotypic vacuolar membrane remodeling (Carter et al., 2004; Martens and McMahon, 2008). In *Arabidopsis*, cell size was shown to be restricted by SNARE-dependent vacuolar morphology mediated through auxin (Löfke et al., 2015). Rapid alkalinization factor (RALF1) is a secreted peptide suppressing cell elongation by activating the cell surface receptor FERONIA in *Arabidopsis thaliana* (Haruta et al., 2014). RALF1 triggers cell wall alkalinization and growth arrest, possibly through the inhibition of plasma membrane H^+-ATPase activity (Wolf and Höfte, 2014). RPT2 is a subunit of the 26S proteasome regulatory particle, and mutation in the *Arabidopsis* paralog AtRPT2a results in enlarged leaves with increased cell size and extended endoreduplication (Kurepa et al., 2009). It is possible that *ROSES1* controls cell expansion directly or indirectly through regulating these rice DEG paralogs.

Premature Leaf Senescence of *roses1* Mutant Results from Elevated Stomatal Density and Aperture

Strikingly, our work showed that *roses1* mutation promotes the stomata density and aperture, which we believe are the causing factors of precocious senescence occurring in *roses1* mutant leaves. Consistently, a parallel study demonstrated that activated expression of an *Arabidopsis* homeobox protein, a homeodomain-START TF belonging to the Class IV Homeodomain-Leucine Zipper TF family, confers elevated drought tolerance with reduced stomatal density (Nakamura et al., 2006; Yu et al., 2008, 2013). Our gene expression profiling analysis identified several DEGs that could be involved in regulating stomata density in leaves, such as rice genes paralogous to *phospholipase D* (*PLD*) (Uraji et al., 2012), *RD20* (Aubert et al., 2010), *MYB44* (Jung et al., 2008), and *RLKs* (Shpak et al., 2005). PLD is shown to be involved in responses to abiotic stress and abscisic acid signaling of guard cells in *Arabidopsis* (Uraji et al., 2012). AtMYB44, as a transcriptional repressor, regulates stomatal movements and plant drought tolerance in *Arabidopsis* (Cominelli et al., 2005; Jung et al., 2008). Endoplasmic reticulum family RLKs have been shown to regulate stomatal patterning and differentiation (Shpak et al., 2005). ROSES1 regulates stomata density, probably via regulating expression of these downstream targets.

In addition, several protein factors have been demonstrated to be involved in the regulation of stomatal opening and closing. *SYR1/PEN1* (*SYP121*), a gene coding for a vesicle trafficking protein, was observed to function in facilitating stomatal opening via activation of the K^+ channel (Eisenach et al., 2012). *Shoot gravitropism 3* (*SGR3*), a putative component of the SNARE complex, was reported to encode the syntaxin of plants 22 (SYP22 syntaxin), function in vacuolar fusion, and control of stomatal opening (Gao et al., 2005). Various components coding for distinct membrane H^+ pumps capable of generating pH gradients have been demonstrated to be involved in regulating stomatal conductance. Ionic equilibrium in guard cells mediated by plasma membrane H^+-ATPase is an essential factor in the regulation of stomatal opening and closing (Palmgren, 2001). In the process of stomata opening, plasma membrane H^+-ATPase acts as a key

protein to activate H^+ efflux from cytosol and hyperpolarize the plasma membrane (Morsomme et al., 2000). Overexpression of *plasma membrane H^+-ATPase 4* (*PMA4*) in tobacco has been shown to increase glucose and fructose content and promote stomatal opening (Zhao et al., 2000). Moreover, cotton plants overexpressing *Thellungiella halophila vacuolar H^+-pyrophosphatase* (*TsVP*) exhibited increased stomatal conductance under non-salt-stressed conditions (Lv et al., 2008). Indeed, the vacuolar H^+-ATPase (V-ATPase) is a highly conserved, membrane-bound multisubunit enzyme complex containing 14 different subunits (Cipriano et al., 2008; Schumacher and Krebs, 2010). Several subunits of the V-ATPase complex were characterized as regulators of stomatal conductance in various plant species (Allen et al., 2000; Baisakh et al., 2012; Ma et al., 2012; Zhang et al., 2013). Our DGE analysis identified several putative targets regulated by *ROSES1*, such as *SAUR* (Spartz et al., 2012), *NGA* (Ballester et al., 2015), *CAX1* (Conn et al., 2011), *SNARE* (Löfke et al., 2015), and *RALF1* (Bergonci et al., 2014), which are directly or indirectly involved in regulation of vesicle trafficking, vacuolar fusion, membrane H^+ pumps, and ionic equilibrium. These downstream targets seem to simultaneously regulate cell expansion and stomatal movement.

In summary, combining EMS-based mutagenesis and map-based cloning, we identified and isolated the *ROSES1* gene that controls the organ size in rice. The *ROSES1* gene encodes a BEL1-like homeobox TF containing a plant-specific POX domain with an unknown function. Our findings, together with further analysis of the functionality of this *ROSES1* gene, will not only generate foundational knowledge for rice plant development but also provide novel strategy of the yield improvement by manipulating the organ size in rice.

Conflict of Interest

The authors declare that there is no conflict of interest.

Supplemental Material Available

Supplemental material for this article is available online.

Acknowledgments

This work was supported by funds from the Application Development Key Project of Chongqing (cstc2015jcyjB0253), the National Science and Technology Key Project of China (2011CB100401), the National Science Fund for Distinguished Young Scholars (30825030), the National Natural Science Foundation of China (31171179, 31471157 and 31461143008), the Advanced Program of Doctoral Fund of the Ministry of Education of China (20110181130009), a Key Project from the Government of Sichuan Province (2013NZ0014), and a Project from the Government of Anhui Province (2012AKKG0739).

References

Aichinger, E., N. Kornet, T. Friedrich, and T. Laux. 2012. Plant stem cell niches. Annu. Rev. Plant Biol. 63:615–636. doi:10.1146/annurev-arplant-042811-105555

Allen, G.J., S.P. Chu, K. Schumacher, C.T. Shimazaki, D. Vafeados, A. Kemper et al. 2000. Alteration of stimulus-specific guard cell calcium oscillations and stomatal closing in *Arabidopsis det3* mutant. Science 289:2338–2342. doi:10.1126/science.289.5488.2338

Altschul, S.F., T.L. Madden, A.A. Schäffer, J. Zhang, Z. Zhang, W. Miller, et al. 1997. Gapped BLAST and PSI-BLAST: A new generation of protein database search programs. Nucleic Acids Res. 25:3389–3402. doi:10.1093/nar/25.17.3389

Anastasiou, E., and M. Lenhard. 2007. Growing up to one's standard. Curr. Opin. Plant Biol. 10:63–69. doi:10.1016/j.pbi.2006.11.002

Arsham, A.M., and T.P. Neufeld. 2006. Thinking globally and acting locally with TOR. Curr. Opin. Cell Biol. 18:589–597. doi:10.1016/j.ceb.2006.09.005

Ashburner, M., C.A. Ball, J.A. Blake, D. Botstein, H. Butler, J.M. Cherry et al. 2000. Gene ontology: Tool for the unification of biology. Nat. Genet. 25:25–29. doi:10.1038/75556

Aubert, Y., D. Vile, M. Pervent, D. Aldon, B. Ranty, T. Simonneau et al. 2010. RD20, a stress-inducible caleosin, participates in stomatal control, transpiration and drought tolerance in *Arabidopsis thaliana*. Plant Cell Physiol. 51:1975–1987. doi:10.1093/pcp/pcq155

Baisakh, N., M.V. RamanaRao, K. Rajasekaran, P. Subudhi, J. Janda, D. Galbraith et al. 2012. Enhanced salt stress tolerance of rice plants expressing a vacuolar H^+-ATPase subunit c1 (*SaVHAc1*) gene from the halophyte grass *Spartina alterniflora* Löisel. Plant Biotechnol. J. 10:453–464. doi:10.1111/j.1467-7652.2012.00678.x

Ballester, P., M. Navarrete-Gómez, P. Carbonero, L. Oñate-Sánchez, and C. Ferrándiz. 2015. Leaf expansion in Arabidopsis is controlled by a TCP-NGA regulatory module likely conserved in distantly related species. Physiol. Plant. 155:21–32. doi:10.1111/ppl.12327

Bao, W.K., and L. Leng. 2005. Determination methods for photosynthetic pigment content of bryophyte with special relation of extraction solvents. Chin. J. Appl. Environ. Biol. 11:235–237.

Barton, M.K. 2010. Twenty years on: The inner workings of the shoot apical meristem, a developmental dynamo. Dev. Biol. 341:95–113. doi:10.1016/j.ydbio.2009.11.029

Bergonci, T., M.C. Silva-Filho, and D.S. Moura. 2014. Antagonistic relationship between AtRALF1 and brassinosteroid regulates cell expansion-related genes. Plant Signal. Behav. 9:e976146. doi:10.4161/15592324.2014.976146

Brand, U., J.C. Fletcher, M. Hobe, E.M. Meyerowitz, and R. Simon. 2000. Dependence of stem cell fate in *Arabidopsis* on a feedback loop regulated by CLV3 activity. Science 289:617–619. doi:10.1126/science.289.5479.617

Bringmann, M., E. Li, A. Sampathkumar, T. Kocabek, M.T. Hauser, and S. Persson. 2012. POM-POM2/cellulose synthase interacting1 is essential for the functional association of cellulose synthase and microtubules in *Arabidopsis*. Plant Cell 24:163–177. doi:10.1105/tpc.111.093575

Cao, L., J.L. Henty-Ridilla, L. Blanchoin, and C.J. Staiger. 2016. Profilin-dependent nucleation and assembly of actin filaments controls cell elongation in *Arabidopsis*. Plant Physiol.

170:220–233. doi:10.1104/pp.15.01321
Carter, C., S. Pan, J. Zouhar, E.L. Avila, T. Girke, and N.V. Raikhel. 2004. The vegetative vacuole proteome of *Arabidopsis thaliana* reveals predicted and unexpected proteins. Plant Cell 16:3285–3303. doi:10.1105/tpc.104.027078
Chen, S.L., H.L. Jia, H.Y. Zhao, D. Liu, Y.M. Liu, B.Y. Liu et al. 2016. Anisotropic cell expansion is affected through the bidirectional mobility of cellulose synthase complexes and phosphorylation at two critical residues on CESA3. Plant Physiol. 171:242–250. doi:10.1104/pp.15.01874
Chen, X., L. Grandont, H. Li, R. Hauschild, S. Paque, A. Abuzeineh et al. 2014. Inhibition of cell expansion by rapid ABP1-mediated auxin effect on microtubules. Nature 516:90–93. doi:10.1038/nature13889
Cho, H.T., and D.J. Cosgrove. 2000. Altered expression of expansin modulates leaf growth and pedicel abscission in *Arabidopsis thaliana*. Proc. Natl. Acad. Sci. USA 97:9783–9788. doi:10.1073/pnas.160276997
Cipriano, D.J., Y. Wang, S. Bond, A. Hinton, K.C. Jefferies, J. Qi, and M. Forgac. 2008. Structure and regulation of the vacuolar ATPases. Biochim. Biophys. Acta, Bioenerg. 1777:599–604. doi:10.1016/j.bbabio.2008.03.013
Cominelli, E., M. Galbiati, A. Vavasseur, L. Conti, T. Sala, M. Vuylsteke et al. 2005. A guard-cell-specific MYB transcription factor regulates stomatal movements and plant drought tolerance. Curr. Biol. 15:1196–1200. doi:10.1016/j.cub.2005.05.048
Conn, S.J., M. Gilliham, A. Athman, A.W. Schreiber, U. Baumann, I. Moller et al. 2011. Cell-specific vacuolar calcium storage mediated by *CAX1* regulates apoplastic calcium concentration, gas exchange, and plant productivity in *Arabidopsis*. Plant Cell 23:240–257. doi:10.1105/tpc.109.072769
Cui, X.H., F.S. Hao, H. Chen, J. Chen, and X.C. Wang. 2008. Expression of the *Vicia faba VfPIP1* gene in *Arabidopsis thaliana* plants improves their drought resistance. J. Plant Res. 121:207–214. doi:10.1007/s10265-007-0130-z
Dinneny, J.R., R. Yadegari, R.L. Fischer, M.F. Yanofsky, and D. Weigel. 2004. The role of *JAGGED* in shaping lateral organs. Development 131:1101–1110. doi:10.1242/dev.00949
Doerks, T., R.R. Copley, J. Schultz, C.P. Ponting, and P. Bork. 2002. Systematic identification of novel protein domain families associated with nuclear functions. Genome Res. 12:47–56. doi:10.1101/gr.203201
Dong, J., G. Feldmann, J. Huang, S. Wu, N. Zhang, S.A. Comerford et al. 2007. Elucidation of a universal size-control mechanism in *Drosophila* and mammals. Cell 130:1120–1133. doi:10.1016/j.cell.2007.07.019
Du, L., N. Li, L.L. Chen, Y.X. Xu, Y. Li, Y.Y. Zhang et al. 2014. The ubiquitin receptor DA1 regulates seed and organ size by modulating the stability of the ubiquitin-specific protease UBP15/SOD2 in *Arabidopsis*. Plant Cell 26:665–677. doi:10.1105/tpc.114.122663
Eisenach, C., Z.H. Chen, C. Grefen, and M.R. Blatt. 2012. The trafficking protein SYP121 of *Arabidopsis* connects programmed stomatal closure and K^+ channel activity with vegetative growth. Plant J. 69:241–251. doi:10.1111/j.1365-313X.2011.04786.x
Fang, L.K., Y.F. Li, X.P. Gong, X.C. Sang, Y.H. Ling, X.W. Wang et al. 2010. Genetic analysis and gene mapping of dominant presenescing leaf gene *PSL3* in rice (*Oryza sativa* L.). Chin. Sci. Bull. 55:2517–2521. doi:10.1007/s11434-010-4013-7
Fletcher, J.C., U. Brand, M.P. Running, R. Simon, and E.M. Meyerowitz. 1999. Signaling of cell fate decisions by *CLAVATA3* in *Arabidopsis* shoot meristems. Science 283:1911–1914. doi:10.1126/science.283.5409.1911
Fujikura, U., L. Elsaesser, H. Breuninger, C. Sánchez-Rodríguez, A. Ivakov, T. Laux et al. 2014. Atkinesin-13A modulates cell-wall synthesis and cell expansion in *Arabidopsis thaliana* via the THESEUS1 pathway. PLoS Genet. 10:e1004627. doi:10.1371/journal.pgen.1004627
Galli, M., and A. Gallavotti. 2016. Expanding the regulatory network for meristem size in plants. Trends Genet. 32:372–383. doi:10.1016/j.tig.2016.04.001
Galva, C., V. Kirik, J.J. Lindeboom, D. Kaloriti, D.M. Rancour, P.J. Hussey et al. 2014. The microtubule plus-end tracking proteins SPR1 and EB1b interact to maintain polar cell elongation and directional organ growth in *Arabidopsis*. Plant Cell 26:4409–4425. doi:10.1105/tpc.114.131482
Gao, X.Q., C.G. Li, P.C. Wei, X.Y. Zhang, J. Chen, and X.C. Wang. 2005. The dynamic changes of tonoplasts in guard cells are important for stomatal movement in *Vicia faba*. Plant Physiol. 139:1207–1216. doi:10.1104/pp.105.067520
Guo, S., T.Q. Zhang, Y.D. Xing, X.Y. Zhu, X.C. Sang, Y.H. Ling et al. 2014. Identification and gene mapping of an early senescence leaf 4 mutant of rice. Crop Sci. 54:2713–2723. doi:10.2135/cropsci2013.12.0854
Ha, C.M., J.H. Jun, and J.C. Fletcher. 2010. Shoot apical meristem form and function. Curr. Top. Dev. Biol. 91:103–140. doi:10.1016/S0070-2153(10)91004-1
Haruta, M., G. Sabat, K. Stecker, B.B. Minkoff, and M.R. Sussman. 2014. A peptide hormone and its receptor protein kinase regulate plant cell expansion. Science 343:408–411. doi:10.1126/science.1244454
Horiguchi, G., G.T. Kim, and H. Tsukaya. 2005. The transcription factor AtGRF5 and the transcription coactivator AN3 regulate cell proliferation in leaf primordia of *Arabidopsis thaliana*. Plant J. 43:68–78. doi:10.1111/j.1365-313X.2005.02429.x
Hu, Y., H.M. Poh, and N.H. Chua. 2006. The *Arabidopsis ARGOS-LIKE* gene regulates cell expansion during organ growth. Plant J. 47:1–9. doi:10.1111/j.1365-313X.2006.02750.x
Hu, Y.X., Q. Xie, and N.H. Chua. 2003. The *Arabidopsis* auxin-inducible gene *ARGOS* controls lateral organ size. Plant Cell 15:1951–1961. doi:10.1105/tpc.013557
Hur, Y.S., J.H. Um, S. Kim, K. Kim, H.J. Park, J.S. Lim et al. 2015. *Arabidopsis thaliana* homeobox 12 (ATHB12), a homeodomain-leucine zipper protein, regulates leaf growth by promoting cell expansion and endoreduplication. New Phytol. 205:316–328. doi:10.1111/nph.12998
Ingram, G.C., and R. Waites. 2006. Keeping it together: Co-ordinating plant growth. Curr. Opin. Plant Biol. 9:12–20. doi:10.1016/j.pbi.2005.11.007
Jefferson, R.A., T.A. Kavanagh, and M.W. Bevan. 1987. GUS fusions: Beta-glucuronidase as a sensitive and versatile gene fusion marker in higher plants. EMBO J. 6:3901–3907.
Jiang, J.J., C. Zhang, and X.L. Wang. 2015. A recently evolved isoform of the transcription factor BES1 promotes brassinosteroid signaling and development in *Arabidopsis thaliana*. Plant Cell 27:361–374. doi:10.1105/tpc.114.133678
Johansson, H., H.J. Jones, J. Foreman, J.R. Hemsted, K. Stewart, R. Grima, and K.J. Halliday. 2014. *Arabidopsis* cell expansion is controlled by a photothermal switch. Nat. Commun. 5:4848. doi:10.1038/ncomms5848
Jung, C., J.S. Seo, S.W. Han, Y.J. Koo, C.H. Kim, S.I. Song et al. 2008. Overexpression of *AtMYB44* enhances stomatal closure to confer abiotic stress tolerance in transgenic *Arabidopsis*. Plant Physiol. 146:623–635. doi:10.1104/pp.107.110981

Kamiya, N., H. Nagasaki, A. Morikami, Y. Sato, and M. Matsuoka. 2003. Isolation and characterization of a rice *WUSCHEL*-type homeobox gene that is specifically expressed in the central cells of a quiescent center in the root apical meristem. Plant J. 35:429–441. doi:10.1046/j.1365-313X.2003.01816.x

Karnik, R., B. Zhang, S. Waghmare, C. Aderhold, C. Grefen, and M.R. Blatt. 2015. Binding of SEC11 indicates its role in SNARE recycling after vesicle fusion and identifies two pathways for vesicular traffic to the plasma membrane. Plant Cell 27:675–694. doi:10.1105/tpc.114.134429

Katano, M., K. Takahashi, T. Hirano, Y. Kazama, T. Abe, H. Tsukaya, and A. Ferjani. 2016. Suppressor screen and phenotype analyses revealed an emerging role of the monofunctional peroxisomal enoyl-CoA hydratase 2 in compensated cell enlargement. Front. Plant Sci. 7:132. doi:10.3389/fpls.2016.00132

Kim, G.T., K. Shoda, T. Tsuge, K.H. Cho, H. Uchimiya, R. Yokoyama et al. 2002. The *ANGUSTIFOLIA* gene of *Arabidopsis*, a plant *CtBP* gene, regulates leaf-cell expansion, the arrangement of cortical microtubules in leaf cells and expression of a gene involved in cell-wall formation. EMBO J. 21:1267–1279. doi:10.1093/emboj/21.6.1267

Kim, G.T., H. Tsukaya, Y. Saito, and H. Uchimiya. 1999. Changes in the shapes of leaves and flowers upon overexpression of cytochrome P450 in *Arabidopsis*. Proc. Natl. Acad. Sci. USA 96:9433–9437. doi:10.1073/pnas.96.16.9433

Kim, G.T., H. Tsukaya, and H. Uchimiya. 1998. The *ROTUNDIFOLIA3* gene of *Arabidopsis thaliana* encodes a new member of the cytochrome P-450 family that is required for the regulated polar elongation of leaf cells. Genes Dev. 12:2381–2391. doi:10.1101/gad.12.15.2381

Kim, J.H., D. Choi, and H. Kende. 2003. The AtGRF family of putative transcription factors is involved in leaf and cotyledon growth in *Arabidopsis*. Plant J. 36:94–104. doi:10.1046/j.1365-313X.2003.01862.x

Kim, J.H., and H. Kende. 2004. A transcriptional coactivator, AtGIF1, is involved in regulating leaf growth and morphology in *Arabidopsis*. Proc. Natl. Acad. Sci. USA 101:13374–13379. doi:10.1073/pnas.0405450101

Kohorn, B.D. 2016. Cell wall-associated kinases and pectin perception. J. Exp. Bot. 67:489–494. doi:10.1093/jxb/erv467

Krizek, B.A. 1999. Ectopic expression of *AINTEGUMENTA* in *Arabidopsis* plants results in increased growth of floral organs. Dev. Genet. 25:224–236. doi:10.1002/(SICI)1520-6408(1999)25:3<224::AID-DVG5>3.0.CO;2-Y

Kumar, S., G. Stecher, and K. Tamura. 2016. MEGA7: Molecular evolutionary genetics analysis version 7.0 for bigger datasets. Mol. Biol. Evol. 33:1870–1874. doi:10.1093/molbev/msw054

Kurepa, J., S. Wang, Y. Li, D. Zaitlin, A.J. Pierce, and J.A. Smalle. 2009. Loss of 26S proteasome function leads to increased cell size and decreased cell number in *Arabidopsis* shoot organs. Plant Physiol. 150:178–189. doi:10.1104/pp.109.135970

Ladwig, F., R.I. Dahlke, N. Stührwohldt, J. Hartmann, K. Harter, and M. Sauter. 2015. Phytosulfokine regulates growth in *Arabidopsis* through a response module at the plasma membrane that includes CYCLIC NUCLEOTIDE-GATED CHANNEL17, H^+-ATPase, and BAK1. Plant Cell 27:1718–1729. doi:10.1105/tpc.15.00306

Li, Y.Y., C. Wang, X.Y. Liu, J. Song, H.J. Li, Z.P. Sui et al. 2016. Up-regulating the abscisic acid inactivation gene *ZmABA8ox1b* contributes to seed germination heterosis by promoting cell expansion. J. Exp. Bot. 67:2889–2900. doi:10.1093/jxb/erw131

Li, Y., L. Zheng, F. Corke, C. Smith, and M.W. Bevan. 2008. Control of final seed and organ size by the *DA1* gene family in *Arabidopsis thaliana*. Genes Dev. 22:1331–1336. doi:10.1101/gad.463608

Liu, T., J. Tian, G.D. Wang, Y.J. Yu, C.F. Wang, Y.P. Ma et al. 2014. Augmin triggers microtubule-dependent microtubule nucleation in interphase plant cells. Curr. Biol. 24:2708–2713. doi:10.1016/j.cub.2014.09.053

Löfke, C., K. Dünser, D. Scheuring, and J. Kleine-Vehn. 2015. Auxin regulates SNARE-dependent vacuolar morphology restricting cell size. eLife 4:e05868. doi:10.7554/eLife.05868

Long, J.A., E.I. Moan, J.I. Medford, and M.K. Barton. 1996. A member of the KNOTTED class of homeodomain proteins encoded by the *STM* gene of *Arabidopsis*. Nature 379:66–69. doi:10.1038/379066a0

Lu, D., T. Wang, S. Persson, B. Mueller-Roeber, and J.H. Schippers. 2014a. Transcriptional control of ROS homeostasis by KUODA1 regulates cell expansion during leaf development. Nat. Commun. 5:3767. doi:10.1038/ncomms4767

Lu, X.D., D.Y. Zhang, S.P. Li, Y.P. Su, Q.J. Liang, H.Y. Meng et al. 2014b. FtsHi4 is essential for embryogenesis due to its influence on chloroplast development in *Arabidopsis*. PLoS One 9:e99741. doi:10.1371/journal.pone.0099741

Luo, Z.K., Z.L. Yang, B.Q. Zhong, Y.F. Li, R. Xie, F.M. Zhao et al. 2007. Genetic analysis and fine mapping of a dynamic rolled leaf gene, *RL10(t)*, in rice (*Oryza sativa* L.). Genome 50:811–817. doi:10.1139/G07-064

Lv, S.L., K.W. Zhang, Q. Gao, L.J. Lian, Y.J. Song, and J.R. Zhang. 2008. Overexpression of an H^+-PPase gene from *Thellungiella halophila* in cotton enhances salt tolerance and improves growth and photosynthetic performance. Plant Cell Physiol. 49:1150–1164. doi:10.1093/pcp/pcn090

Ma, B.Y., D. Qian, Q. Nan, C. Tan, L.Z. An, and Y. Xiang. 2012. Arabidopsis vacuolar H^+-ATPase (V-ATPase) B subunits are involved in actin cytoskeleton remodeling via binding to, bundling, and stabilizing F-actin. J. Biol. Chem. 287:19008–19017. doi:10.1074/jbc.M111.281873

Martens, S., and H.T. McMahon. 2008. Mechanisms of membrane fusion: Disparate players and common principles. Nat. Rev. Mol. Cell Biol. 9:543–556. doi:10.1038/nrm2417

Martinez-Fernandez, I., S. Sanchís, N. Marini, V. Balanzá, P. Ballester, M. Navarrete-Gómez et al. 2014. The effect of NGATHA altered activity on auxin signaling pathways within the *Arabidopsis gynoecium*. Front. Plant Sci. 5:210.

Mayer, K.F., H. Schoof, A. Haecker, M. Lenhard, G. Jürgens, and T. Laux. 1998. Role of *WUSCHEL* in regulating stem cell fate in the *Arabidopsis* shoot meristem. Cell 95:805–815. doi:10.1016/S0092-8674(00)81703-1

McCouch, S.R., L. Teytelman, Y. Xu, K.B. Lobos, K. Clare, M. Walton, et al. 2002. Development and mapping of 2240 new SSR markers for rice (*Oryza sativa* L.). DNA Res. 9:199–207. doi:10.1093/dnares/9.6.199

Media Cybernetics. 2006. ImageProPlus software. Release 6.0. Media Cybernetics, Rockville, MD.

Michelmore, R.W., I. Paran, and R.V. Kesseli. 1991. Identification of markers linked to disease-resistance genes by bulked segregant analysis: A rapid method to detect markers in specific genomic regions by using segregating populations. Proc. Natl. Acad. Sci. USA 88:9828–9832. doi:10.1073/pnas.88.21.9828

Mizukami, Y. 2001. A matter of size: Developmental control of organ size in plants. Curr. Opin. Plant Biol. 4:533–539. doi:10.1016/S1369-5266(00)00212-0

Mizukami, Y., and R.L. Fischer. 2000. Plant organ size control:

AINTEGUMENTA regulates growth and cell numbers during organogenesis. Proc. Natl. Acad. Sci. USA 97:942–947.
Morsomme, P., C.W. Slayman, and A. Goffeau. 2000. Mutagenic study of the structure, function and biogenesis of the yeast plasma membrane H(+)-ATPase. Biochim. Biophys. Acta 1469:133–157. doi:10.1016/S0304-4157(00)00015-0
Mouille, G., M.C. Ralet, C. Cavelier, C. Eland, D. Effroy, K. Hématy et al. 2007. Homogalacturonan synthesis in *Arabidopsis thaliana* requires a Golgi-localized protein with a putative methyltransferase domain. Plant J. 50:605–614. doi:10.1111/j.1365-313X.2007.03086.x
Murray, M.G., and W.F. Thompson. 1980. Rapid isolation of high molecular weight plant DNA. Nucleic Acids Res. 8:4321–4326. doi:10.1093/nar/8.19.4321
Nakajima, K., I. Furutani, H. Tachimoto, H. Matsubara, and T. Hashimoto. 2004. *SPIRAL1* encodes a plant-specific microtubule-localized protein required for directional control of rapidly expanding Arabidopsis cells. Plant Cell 16:1178–1190. doi:10.1105/tpc.017830
Nakamura, M., H. Katsumata, M. Abe, N. Yabe, Y. Komeda, K.T. Yamamoto, and T. Takahashi. 2006. Characterization of the class IV homeodomain-leucine zipper gene family in *Arabidopsis*. Plant Physiol. 141:1363–1375. doi:10.1104/pp.106.077388
Nath, U., B.C. Crawford, R. Carpenter, and E. Coen. 2003. Genetic control of surface curvature. Science 299:1404–1407. doi:10.1126/science.1079354
Ohno, C.K., G.V. Reddy, M.G. Heisler, and E.M. Meyerowitz. 2004. The *Arabidopsis JAGGED* gene encodes a zinc finger protein that promotes leaf tissue development. Development 131:1111–1122. doi:10.1242/dev.00991
Palmgren, M.G. 2001. Plant plasma membrane H^+-ATPase: Powerhouses for nutrient up take. Annu. Rev. Plant Physiol. Plant Mol. Biol. 52:817–845. doi:10.1146/annurev.arplant.52.1.817
Pan, D. 2007. Hippo signaling in organ size control. Genes Dev. 21:886–897. doi:10.1101/gad.1536007
Paque, S., G. Mouille, L. Grandont, D. Alabadí, C. Gaertner, A. Goyallon et al. 2014. AUXIN BINDING PROTEIN1 links cell wall remodeling, auxin signaling, and cell expansion in *Arabidopsis*. Plant Cell 26:280–295. doi:10.1105/tpc.113.120048
Park, J., Y. Cui, and B.H. Kang. 2015. AtPGL3 is an *Arabidopsis* BURP domain protein that is localized to the cell wall and promotes cell enlargement. Front. Plant Sci. 6:412. doi:10.3389/fpls.2015.00412
Pearce, G., D.S. Moura, J. Stratmann, and C.A. Ryan. 2001. RALF, a 5-kDa ubiquitous polypeptide in plants, arrests root growth and development. Proc. Natl. Acad. Sci. USA 98:12843–12847. doi:10.1073/pnas.201416998 [erratum: 98(22):12843].
Peremyslov, V.V., R.A. Cole, J.E. Fowler, and V.V. Dolja. 2015. Myosin-powered membrane compartment drives cytoplasmic streaming, cell expansion and plant development. PLoS One 10:e0139331. doi:10.1371/journal.pone.0139331
Polko, J.K., J.A. van Rooij, S. Vanneste, R. Pierik, A.M. Ammerlaan, M.H. Vergeer-van Eijk et al. 2015. Ethylene-mediated regulation of A2-Type CYCLINs modulates hyponastic growth in *Arabidopsis*. Plant Physiol. 169:194–208. doi:10.1104/pp.15.00343
Qin, Z.X., X. Zhang, X.R. Zhang, G.P. Feng, and Y.X. Hu. 2014. The Arabidopsis *ORGAN SIZE RELATED 2* is involved in regulation of cell expansion during organ growth. BMC Plant Biol. 14:349. doi:10.1186/s12870-014-0349-5
Raggi, S., A. Ferrarini, M. Delledonne, C. Dunand, P. Ranocha, G. De Lorenzo et al. 2015. The *Arabidopsis* class III peroxidase AtPRX71 negatively regulates growth under physiological conditions and in response to cell wall damage. Plant Physiol. 169:2513–2525.
Randall, R.S., E. Sornay, W. Dewitte, and J.A. Murray. 2015. *AINTEGUMENTA* and the D-type cyclin *CYCD3;1* independently contribute to petal size control in *Arabidopsis*: Evidence for organ size compensation being an emergent rather than a determined property. J. Exp. Bot. 66:3991–4000. doi:10.1093/jxb/erv200
Rao, Y.C., Y.L. Yang, J. Xu, X.J. Li, Y.J. Leng, L.P. Dai et al. 2015. *EARLY SENESCENCE1* encodes a SCAR-LIKE PROTEIN2 that affects water loss in rice. Plant Physiol. 169:1225–1239. doi:10.1104/pp.15.00991
Reddy, G.V., and E.M. Meyerowitz. 2005. Stem-cell homeostasis and growth dynamics can be uncoupled in the *Arabidopsis* shoot apex. Science 310:663–667. doi:10.1126/science.1116261
Ren, D.Y., Y.F. Li, F.M. Zhao, X.C. Sang, J.Q. Shi, N. Wang et al. 2013. *MULTI-FLORET SPIKELET1*, which encodes an AP2/ERF protein, determines spikelet meristem fate and sterile lemma identity in rice. Plant Physiol. 162:872–884. doi:10.1104/pp.113.216044
Rubio-Díaz, S., J.M. Pérez-Pérez, R. González-Bayón, R. Muñoz-Viana, N. Borrega, G. Mouille et al. 2012. Cell expansion-mediated organ growth is affected by mutations in three *EXIGUA* genes. PLoS One 7:e36500. doi:10.1371/journal.pone.0036500
Sang, X.C., Z.L. Yang, B.Q. Zhong, Y.F. Li, L. Hou, Y. Pei et al. 2006. Assessment of purity of rice CMS lines using cpDNA marker. Euphytica 152:177–183. doi:10.1007/s10681-006-9196-2
Sasidharan, R., C.C. Chinnappa, M. Staal, J.T. Elzenga, R. Yokoyama, K. Nishitani et al. 2010. Light quality-mediated petiole elongation in *Arabidopsis* during shade avoidance involves cell wall modification by xyloglucan endotransglucosylase/hydrolases. Plant Physiol. 154:978–990. doi:10.1104/pp.110.162057
Sato, Y., S.K. Hong, A. Tagiri, H. Kitano, N. Yamamoto, Y. Nagato, and M. Matsuoka. 1996. A rice homeobox gene, *OSH1*, is expressed before organ differentiation in a specific region during early embryogenesis. Proc. Natl. Acad. Sci. USA 93:8117–8122. doi:10.1073/pnas.93.15.8117
Schmidt, R., J.H. Schippers, D. Mieulet, T. Obata, A.R. Fernie, E. Guiderdoni, and B. Mueller-Roeber. 2013. Multipass, a rice R2R3-type MYB transcription factor, regulates adaptive growth by integrating multiple hormonal pathways. Plant J. 76:258–273. doi:10.1111/tpj.12286
Schoof, H., M. Lenhard, A. Haecker, K.F. Mayer, G. Jürgens, and T. Laux. 2000. The stem cell population of *Arabidopsis* shoot meristems in maintained by a regulatory loop between the *CLAVATA* and *WUSCHEL* genes. Cell 100:635–644. doi:10.1016/S0092-8674(00)80700-X
Schumacher, K., and M. Krebs. 2010. The V-ATPase: Small cargo, large effects. Curr. Opin. Plant Biol. 13:724–730. doi:10.1016/j.pbi.2010.07.003
Shi, Z.Y., J. Wang, X.S. Wan, G.Z. Shen, X.Q. Wang, and J.L. Zhang. 2007. Over-expression of rice *OsAGO7* gene induces

upward curling of the leaf blade that enhanced erect-leaf habit. Planta 226:99–108. doi:10.1007/s00425-006-0472-0

Shpak, E.D., J.M. McAbee, L.J. Pillitteri, and K.U. Torii. 2005. Stomatal patterning and differentiation by synergistic interactions of receptor kinases. Science 309:290–293. doi:10.1126/science.1109710

Sonoda, Y., K. Sako, Y. Maki, N. Yamazaki, H. Yamamoto, A. Ikeda, and J. Yamaguchi. 2009. Regulation of leaf organ size by the *Arabidopsis* RPT2a 19S proteasome subunit. Plant J. 60:68–78. doi:10.1111/j.1365-313X.2009.03932.x

Spartz, A.K., S.H. Lee, J.P. Wenger, N. Gonzalez, H. Itoh, D. Inzé et al. 2012. The *SAUR19* subfamily of *SMALL AUXIN UP RNA* genes promote cell expansion. Plant J. 70:978–990. doi:10.1111/j.1365-313X.2012.04946.x

Spartz, A.K., H. Ren, M.Y. Park, K.N. Grandt, S.H. Lee, A.S. Murphy et al. 2014. SAUR inhibition of PP2C-D phosphatases activates plasma membrane H^+-ATPases to promote cell expansion in *Arabidopsis*. Plant Cell 26:2129–2142. doi:10.1105/tpc.114.126037

Su, L., C. Bassa, C. Audran, I. Mila, C. Cheniclet, C. Chevalier et al. 2014. The auxin *Sl-IAA17* transcriptional repressor controls fruit size via the regulation of endoreduplication-related cell expansion. Plant Cell Physiol. 55:1969–1976. doi:10.1093/pcp/pcu124

Sugimoto-Shirasu, K., and K. Roberts. 2003. "Big it up": Endoreduplication and cell-size control in plants. Curr. Opin. Plant Biol. 6:544–553. doi:10.1016/j.pbi.2003.09.009

Szécsi, J., C. Joly, K. Bordji, E. Varaud, J.M. Cock, C. Dumas, and M. Bendahmane. 2006. *BIGPETALp*, a *bHLH* transcription factor is involved in the control of *Arabidopsis* petal size. EMBO J. 25:3912–3920. doi:10.1038/sj.emboj.7601270

Tanaka, W., Y. Ohmori, T. Ushijima, H. Matsusaka, T. Matsushita, T. Kumamaru et al. 2015. Axillary meristem formation in rice requires the *WUSCHEL* ortholog *TILLERS ABSENT1*. Plant Cell 27:1173–1184. doi:10.1105/tpc.15.00074

Testone, G., E. Condello, E. Di Giacomo, C. Nicolodi, E. Caboni, A. Rasori et al. 2015. The *KNOTTED*-like genes of peach (*Prunus persica* L. Batsch) are differentially expressed during drupe growth and the class 1 *KNOPE1* contributes to mesocarp development. Plant Sci. 237:69–79. doi:10.1016/j.plantsci.2015.05.005

Tinland, B. 1996. The integration of T-DNA into plant genomes. Trends Plant Sci. 1:178–184. doi:10.1016/1360-1385(96)10020-0

Trapnell, C., L. Pachter, and S.L. Salzberg. 2009. TopHat: Discovering splice junctions with RNA-Seq. Bioinformatics 25:1105–1111. doi:10.1093/bioinformatics/btp120

Trigueros, M., M. Navarrete-Gómez, S. Sato, S.K. Christensen, S. Pelaz, D. Weigel et al. 2009. The *NGATHA* genes direct style development in the *Arabidopsis* gynoecium. Plant Cell 21:1394–1409. doi:10.1105/tpc.109.065508

Tsuda, K., Y. Ito, Y. Sato, and N. Kurata. 2011. Positive autoregulation of a *KNOX* gene is essential for shoot apical meristem maintenance in rice. Plant Cell 23:4368–4381. doi:10.1105/tpc.111.090050

Tsuge, T., H. Tsukaya, and H. Uchimiya. 1996. Two independent and polarized processes of cell elongation regulate leaf blade expansion in *Arabidopsis thaliana* (L.) Heynh. Development 122:1589–1600.

Tsukaya, H. 2003. Organ shape and size: A lesson from studies of leaf morphogenesis. Curr. Opin. Plant Biol. 6:57–62. doi:10.1016/S1369526602000055

Tsukaya, H., and G.T. Beemster. 2006. Genetics, cell cycle and cell expansion in organogenesis in plants. J. Plant Res. 119:1–4. doi:10.1007/s10265-005-0254-y

Uraji, M., T. Katagiri, E. Okuma, W. Ye, M.A. Hossain, C. Masuda et al. 2012. Cooperative function of PLDδ and PLDα1 in abscisic acid-induced stomatal closure in *Arabidopsis*. Plant Physiol. 159:450–460. doi:10.1104/pp.112.195578

van der Graaff, E., T. Laux, and S.A. Rensing. 2009. The WUS homeobox-containing (WOX) protein family. Genome Biol. 10:248. doi:10.1186/gb-2009-10-12-248

Van Dingenen, J., L. De Milde, M. Vermeersch, K. Maleux, R. De Rycke, M. De Bruyne et al. 2016. Chloroplasts are central players in sugar-induced leaf growth. Plant Physiol. 171:590–605. doi:10.1104/pp.15.01669

Vercruyssen, L., V.B. Tognetti, N. Gonzalez, D.J. Van, M.L. De, A. Bielach et al. 2015. GROWTH REGULATING FACTOR5 stimulates *Arabidopsis* chloroplast division, photosynthesis, and leaf longevity. Plant Physiol. 167:817–832. doi:10.1104/pp.114.256180

Wang, Q.L., X.J. Xue, Y.L. Li, Y.B. Dong, L. Zhang, Q. Zhou et al. 2016a. A maize ADP-ribosylation factor *ZmArf2* increases organ and seed size by promoting cell expansion in *Arabidopsis*. Physiol. Plant. 156:97–107. doi:10.1111/ppl.12359

Wang, Z., N. Li, S. Jiang, N. Gonzalez, X. Huang, Y. Wang et al. 2016b. SCF^{SAP} controls organ size by targeting PPD proteins for degradation in *Arabidopsis thaliana*. Nat. Commun. 7:11192. doi:10.1038/ncomms11192

Ware, D., P. Jaiswal, J. Ni, X. Pan, K. Chang, K. Clark, et al. 2002. Gramene: A resource for comparative grass genomics. Nucleic Acids Res. 30:103–105. doi:10.1093/nar/30.1.103

Weraduwage, S.M., S.J. Kim, L. Renna, F.C. Anozie, T.D. Sharkey, and F. Brandizzi. 2016. Pectin methylesterification impacts the relationship between photosynthesis and plant growth. Plant Physiol. 171:833–848.

White, D.W. 2006. *PEAPOD* regulates lamina size and curvature in *Arabidopsis*. Proc. Natl. Acad. Sci. USA 103:13238–13243. doi:10.1073/pnas.0604349103

Wolf, S., and H. Höfte. 2014. Growth control: A saga of cell walls, ROS, and peptide receptors. Plant Cell 26:1848–1856. doi:10.1105/tpc.114.125518

Wolf, S., D. van der Does, F. Ladwig, C. Sticht, A. Kolbeck, A.K. Schürholz et al. 2014. A receptor-like protein mediates the response to pectin modification by activating brassinosteroid signaling. Proc. Natl. Acad. Sci. USA 111:15261–15266. doi:10.1073/pnas.1322979111

Wu, G., J.S. Carville, and E.P. Spalding. 2016. ABCB19-mediated polar auxin transport modulates *Arabidopsis* hypocotyl elongation and the endoreplication variant of the cell cycle. Plant J. 85:209–218. doi:10.1111/tpj.13095

Xia, T., N. Li, J. Dumenil, J. Li, A. Kamenski, M.W. Bevan, F. Gao, and Y. Li. 2013. The ubiquitin receptor DA1 interacts with the E3 ubiquitin ligase DA2 to regulate seed and organ size in *Arabidopsis*. Plant Cell 25:3347–3359. doi:10.1105/tpc.113.115063

Xiao, F., P. Giavalisco, and G.B. Martin. 2007. *Pseudomonas syringae* type III effector AvrPtoB is phosphorylated in plant cells on serine 258, promoting its virulence activity. J. Biol. Chem. 282:30737–30744. doi:10.1074/jbc.M705565200

Xu, R., and Y. Li. 2011. Control of final organ size by mediator complex subunit 25 in *Arabidopsis thaliana*. Development 138:4545–4554. doi:10.1242/dev.071423

Xue, J.S., D.X. Luo, D.Y. Xu, M.H. Zeng, X.F. Cui, L.G. Li,

and H. Huang. 2015. CCR1, an enzyme required for lignin biosynthesis in *Arabidopsis*, mediates cell proliferation exit for leaf development. Plant J. 83:375–387. doi:10.1111/tpj.12902

Yadav, R.K., M. Tavakkoli, and G.V. Reddy. 2010. WUSCHEL mediates stem cell homeostasis by regulating stem cell number and patterns of cell division and differentiation of stem cell progenitors. Development 137:3581–3589. doi:10.1242/dev.054973

Yang, R.F., Q.C. Tang, H.M. Wang, X.B. Zhang, G. Pan, and J.M. Tu. 2011. Analyses of two rice (*Oryza sativa*) cyclin-dependent kinase inhibitors and effects of transgenic expression of *OsiICK6* on plant growth and development. Ann. Bot. (Lond.) 107:1087–1101. doi:10.1093/aob/mcr057

Yano, D., M. Sato, C. Saito, M.H. Sato, M.T. Morita, and M. Tasaka. 2003. A SNARE complex containing SGR3/AtVAM3 and ZIG/VTI11 in gravity-sensing cells is important for *Arabidopsis* shoot gravitropism. Proc. Natl. Acad. Sci. USA 100:8589–8594. doi:10.1073/pnas.1430749100

Yu, H., X. Chen, Y.Y. Hong, Y. Wang, P. Xu, S.D. Ke et al. 2008. Activated expression of an *Arabidopsis* HD-START protein confers drought tolerance with improved root system and reduced stomatal density. Plant Cell 20:1134–1151. doi:10.1105/tpc.108.058263

Yu, L.H., X. Chen, Z. Wang, S.M. Wang, Y.P. Wang, Q.S. Zhu et al. 2013. Arabidopsis *enhanced drought tolerance1/HOMEODOMAIN GLABROUS11* confers drought tolerance in transgenic rice without yield penalty. Plant Physiol. 162:1378–1391. doi:10.1104/pp.113.217596

Zeng, Q., and W.J. Hong. 2008. The emerging role of the hippo pathway in cell contact inhibition, organ size control, and cancer development in mammals. Cancer Cell 13:188–192. doi:10.1016/j.ccr.2008.02.011

Zhang, H.Y., X.L. Niu, J. Liu, F.M. Xiao, S.Q. Cao, and Y.S. Liu. 2013. RNAi-directed downregulation of vacuolar H^+-ATPase subunit a results in enhanced stomatal aperture and density in rice. PLoS One 8:e69046. doi:10.1371/journal.pone.0069046

Zhang, L., S.S. Xiao, W.Q. Li, W. Feng, J. Li, Z.D. Wu et al. 2011. Overexpression of a harpin-encoding gene *hrf1* in rice enhances drought tolerance. J. Exp. Bot. 62:4229–4238. doi:10.1093/jxb/err131

Zhang, X.Q., P.C. Wei, Y.M. Xiong, Y. Yang, J. Chen, and X.C. Wang. 2010. Overexpression of the *Arabidopsis* α-expansin gene, *atexpa1*, accelerates stomatal opening by decreasing the volumetric elastic modulus. Plant Cell Rep. 30:27–36. doi:10.1007/s00299-010-0937-2

Zhao, R., V. Dielen, J.M. Kinet, and M. Boutry. 2000. Cosuppression of a plasma membrane H^+-ATPase isoform impairs sucrose translocation, stomatal opening, plant growth, and male fertility. Plant Cell 12:535–546. doi:10.2307/3871067

Zhao, Y., Y.F. Hu, M.Q. Dai, L.M. Huang, and D.X. Zhou. 2009. The WUSCHEL-related homeobox gene *WOX11* is required to activate shoot-borne crown root development in rice. Plant Cell 21:736–748. doi:10.1105/tpc.108.061655

Zhu, C., A. Ganguly, T.I. Baskin, D.D. McClosky, C.T. Anderson, C. Foster et al. 2015. The fragile Fiber1 kinesin contributes to cortical microtubule-mediated trafficking of cell wall components. Plant Physiol. 167:780–792. doi:10.1104/pp.114.251462